Metodologie e tecnologie per lo sviluppo di un nuovo velivolo

25 ottobre 2014

Le tecnologie innovative per i velivoli di nuova generazione

AERODINAMICA

G. Mingione – (CIRA)

PRELIMINARY DESIGN

$W_{FUEL} = f (W_{MTOW}, Range, E)$ $W_{MTOW} = W_{EMPTY} + W_{FUEL}$

- $W_{EMPTY} = f_1(geometry, W_{MTOW})$
- $E = f_2(geometry)$ (Efficienza aerodinamica)

GEOMETRY

- Wing span
- Aspect ratio
- Wing surface
- ….

CORRELAZIONI SEMIEMPRICHE SONO RICHIESTE PER:

Peso in funzione delle caratteristiche geometriche

Aerodinamica in funzione delle caratteristiche geometriche

COMPITO DELL'AERODINAMICA DURANTE LO SVILUPPO DI UN NUOVO PROGETTO:

DIMOSTRARE CHE LE ASSUNZIONI FATTE NELLA FASE DI DISEGNO PRELIMINARE SIANO REALISTICHE

DEFINIRE LE FORME SUPERFICIALI ESTERNI CAPACI DI SODDISAFARE I REQUISITI AERODINAMICI

FORNIRE DATI AERODINAMICI ALLE ALTRE DISCIPLINE:

Data-base aerodinamico => Meccanica del volo

Carichi aerodinamici => struttura

AERODINAMICA

- ✓ **MASSIMIZZAZIONE EFFICIENZA (RIDUZIONE DELLA RESISTENZA)**
- ✓ **PORTANZA AL DECOLLO**

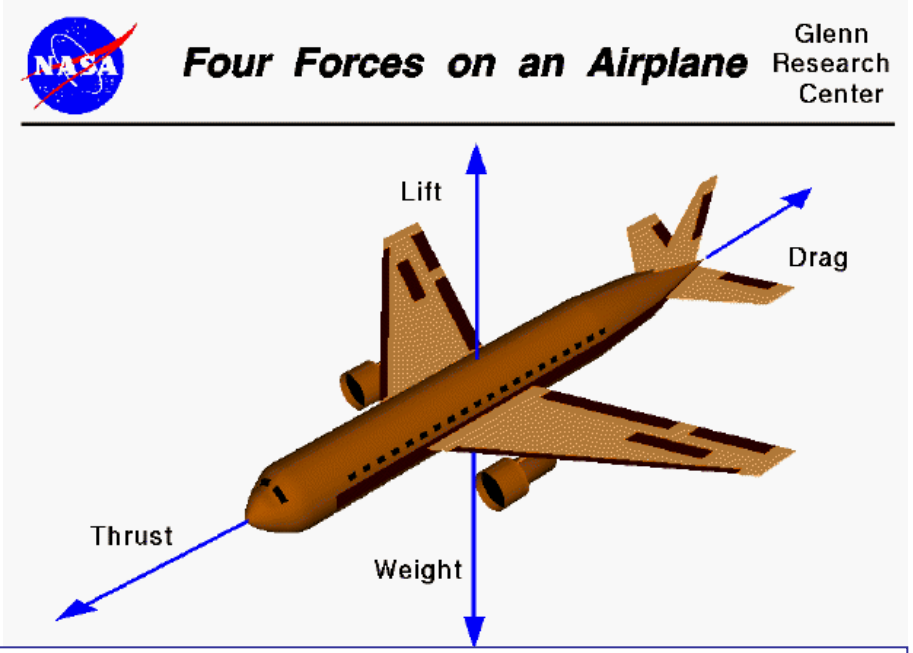

Lift: portanza
Drag: resistenza
Weight: peso
Aerodynamic center: fuoco (diverso dal centro di pressione)
Angle of attack: angolo d'attacco

$$Lift = .5 * Cl * ro * V*V*S$$
$$Drag = .5 * Cd * ro * V*V*S$$
$$Moment = .5 * Cl * ro * V*V*S*c$$

RESISTENZA AERODINAMICA

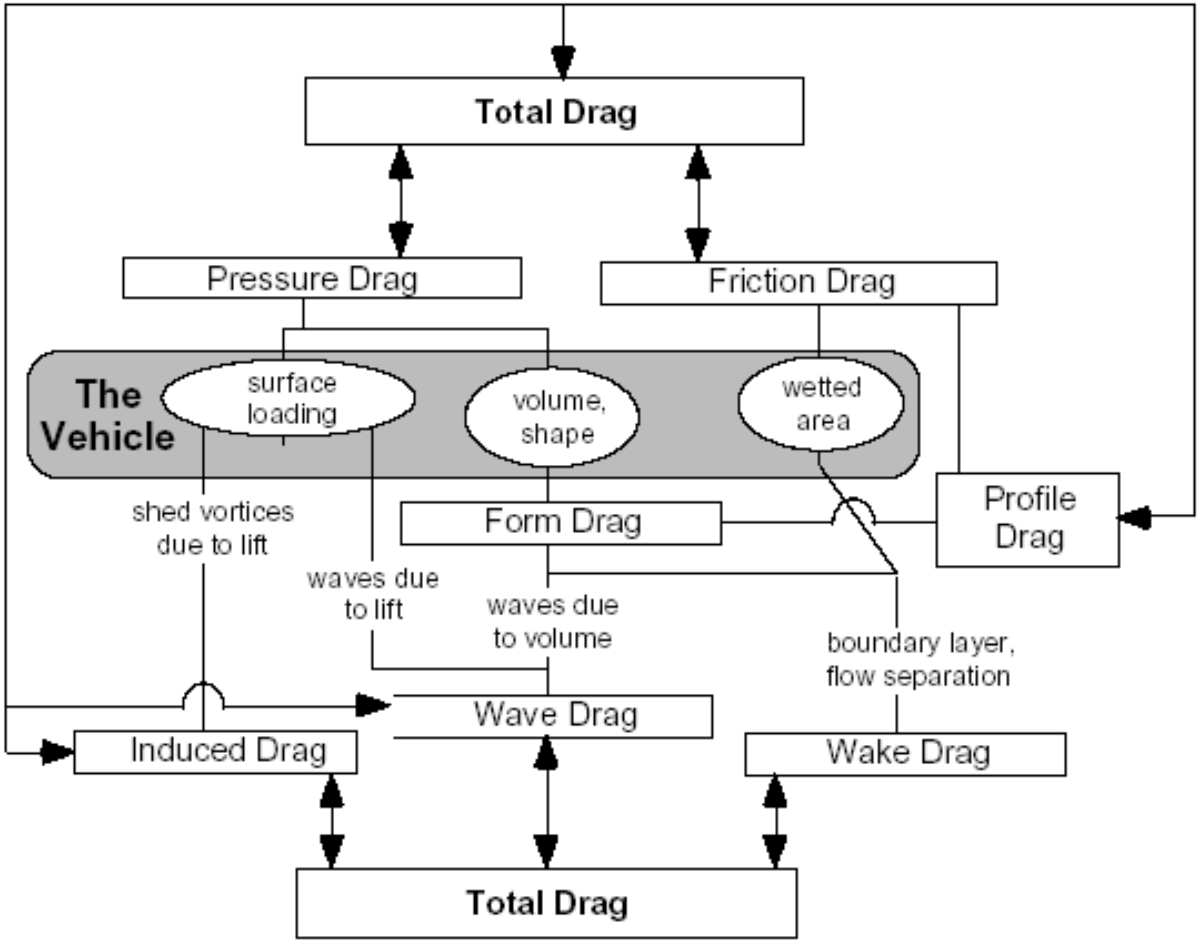

AERODINAMICA

RESISTENZA

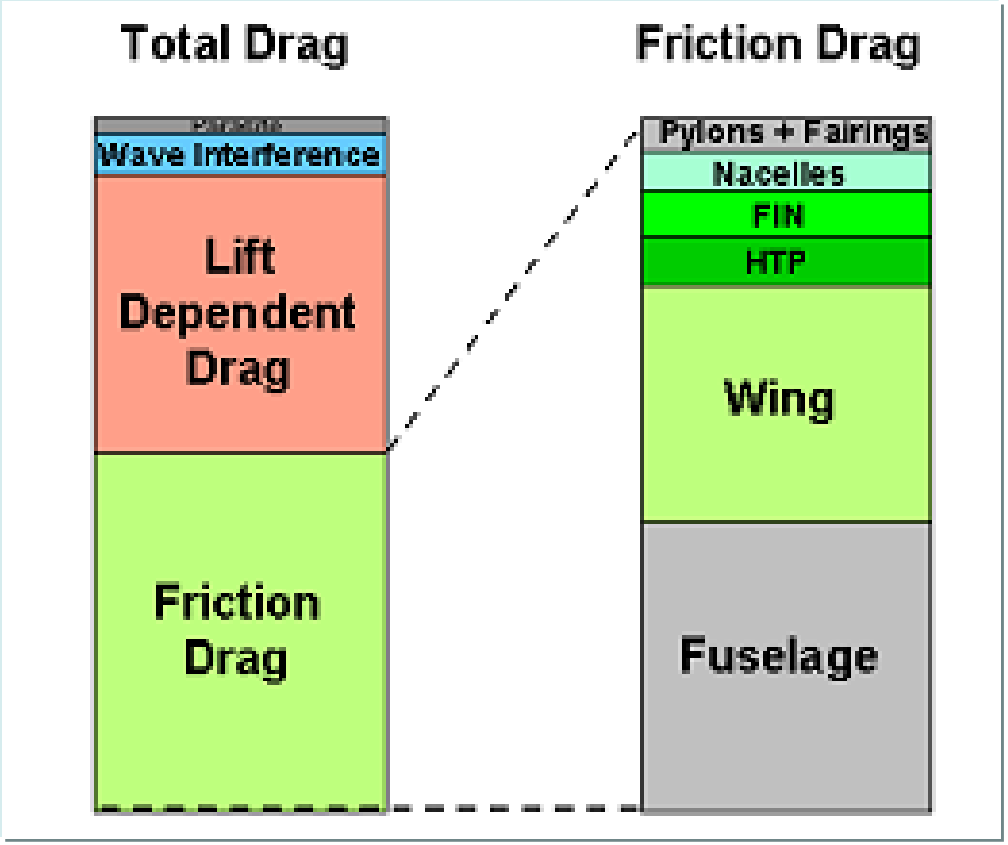

Resistenza d'onda minima se il velivolo é ben disegnato

La resistenza d'onda dipende dalla distribuzione di carico

La resistenza d'attrito dipende principalmente dalla superficie bagnata

AERODINAMICA

RESISTENZA D'ONDA

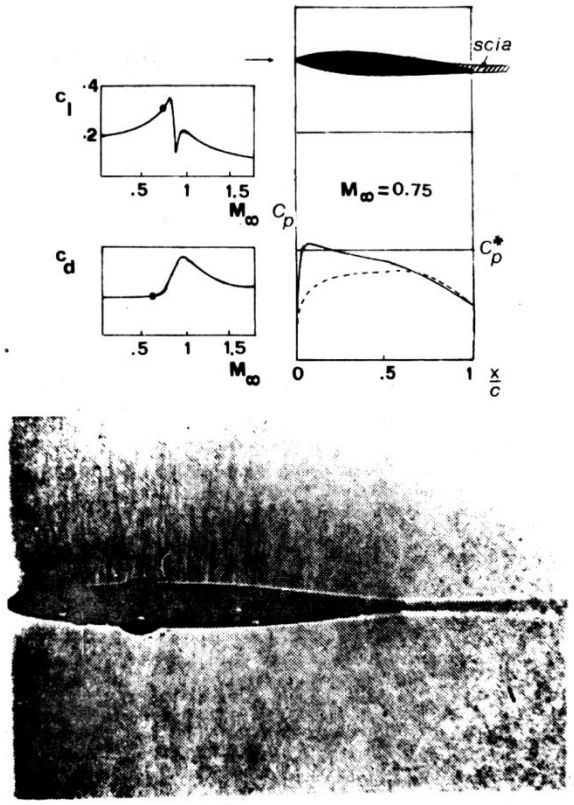

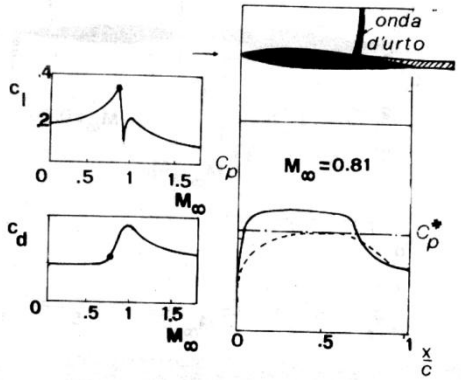

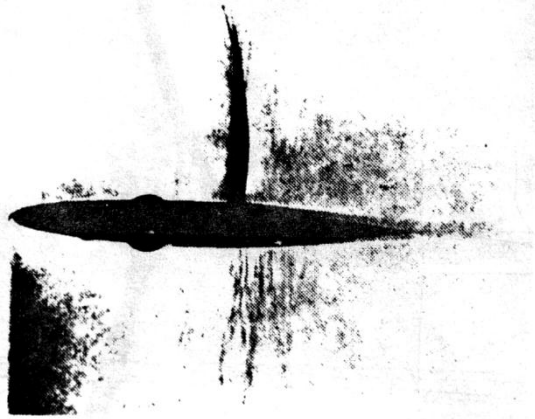

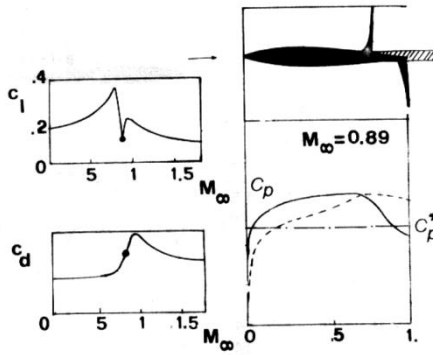

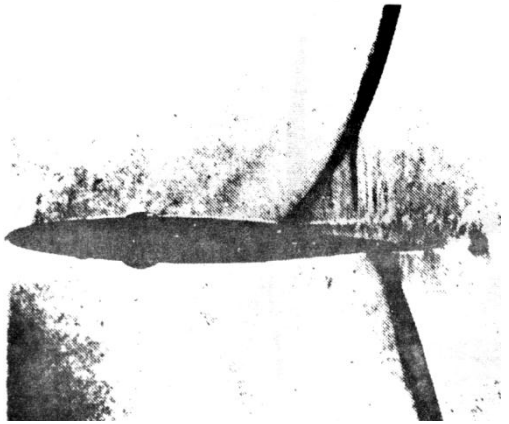

AERODINAMICA

RESISTENZA INDOTTA

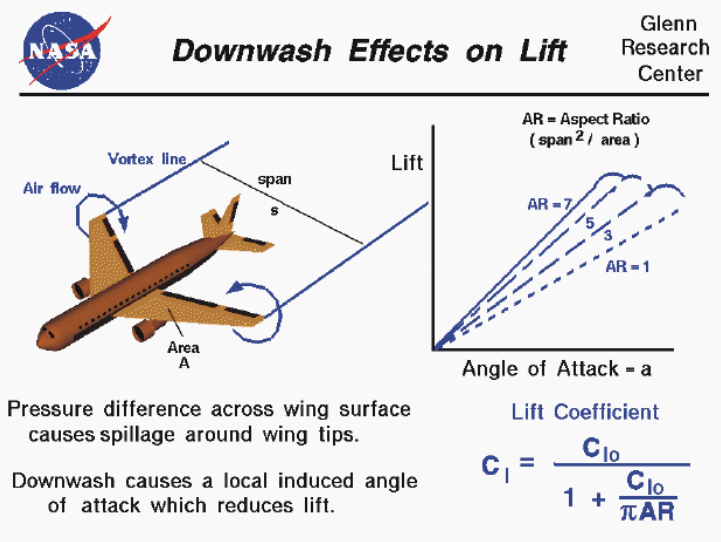

La portanza é ortogonale alla velocità

Il down-wash causa un angolo d'attacco effettivo ridotto e la portanza sarà normale alla velocità effettiva con una componente di resistenza

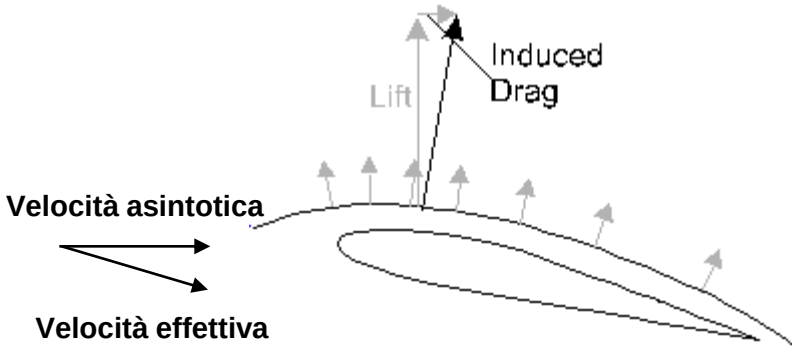

AERODINAMICA: RESISTENZA INDOTTA

Riduzione della resistenza indotta attraverso la forma dell'estremità alare

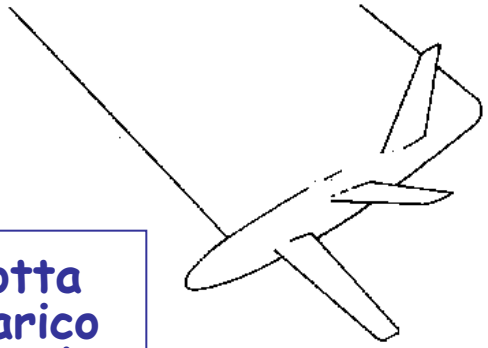

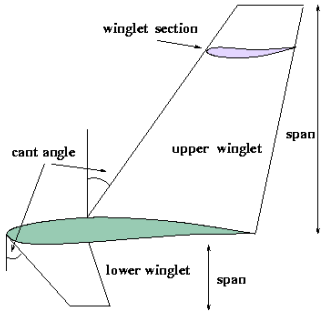

Riduzione della resistenza indotta attraverso ottimizzazione del carico alare nelle diverse condizioni di volo

- ✓ Deformazione ala
- ✓ Variazione del carico causato dal consumo di combustibile

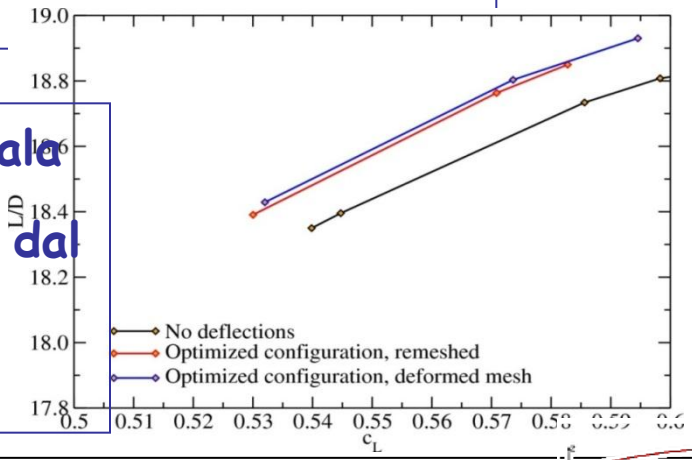

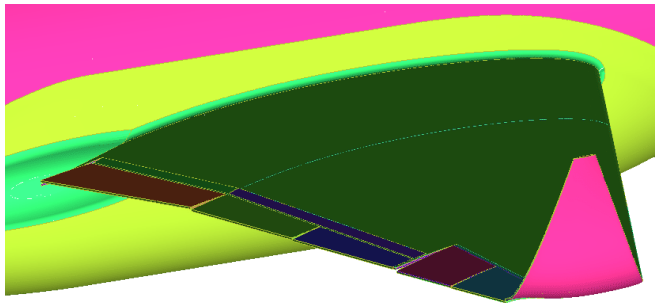

Wing body configuration with flaps and ailerons

Performance at cruise, initial and optimize configuration 1% improvements

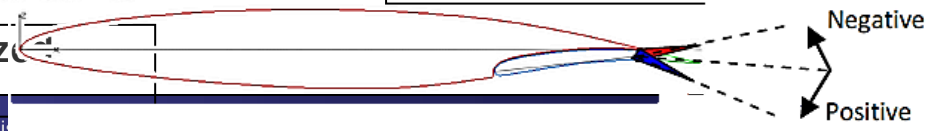

La presenza della parete tende a rallentare il flusso e quindi a creare zone in cui gli effetti viscosi sono predominanti

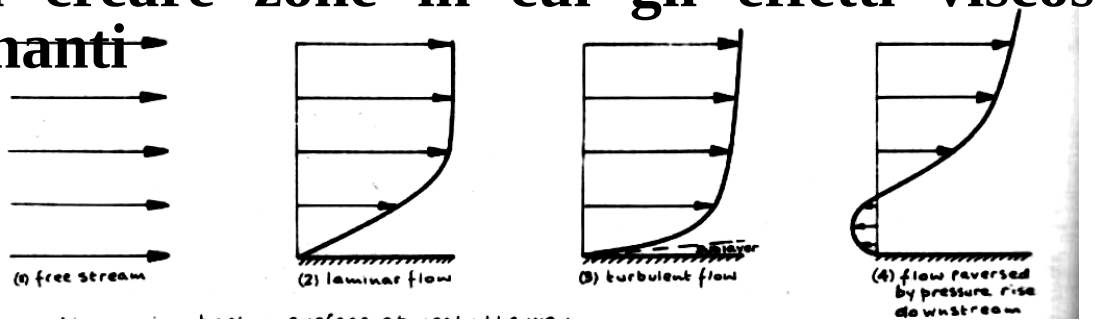

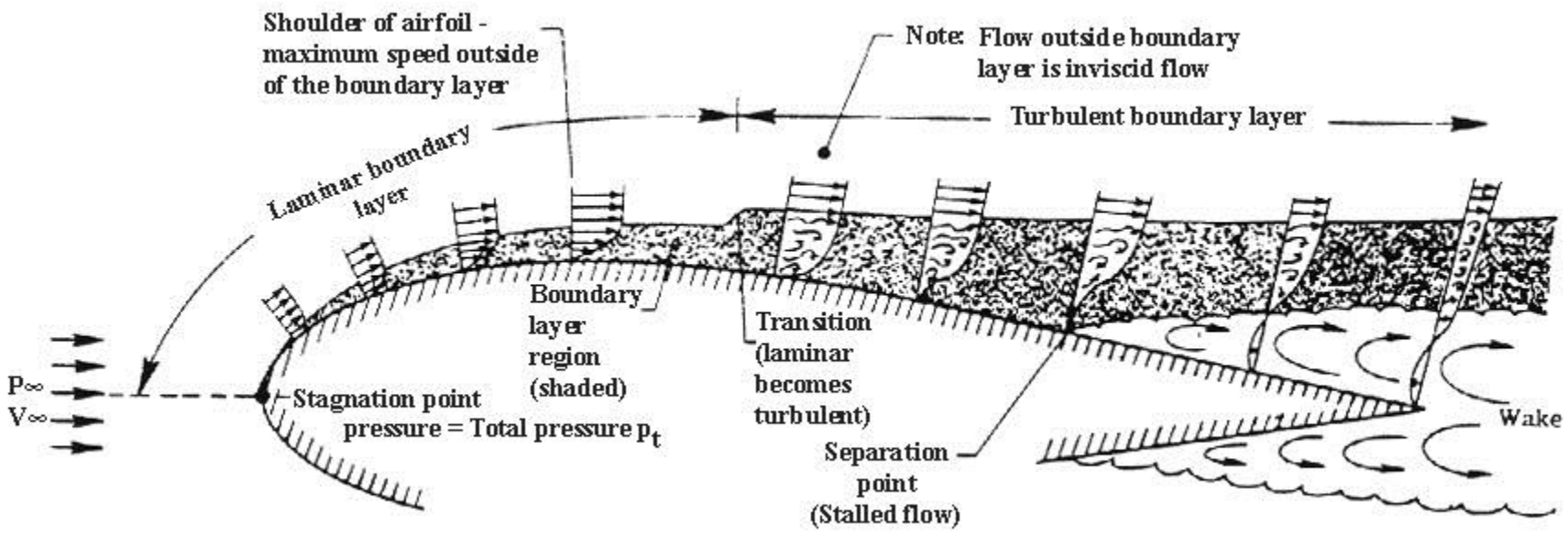

Il numero di Reynolds: Strato limite

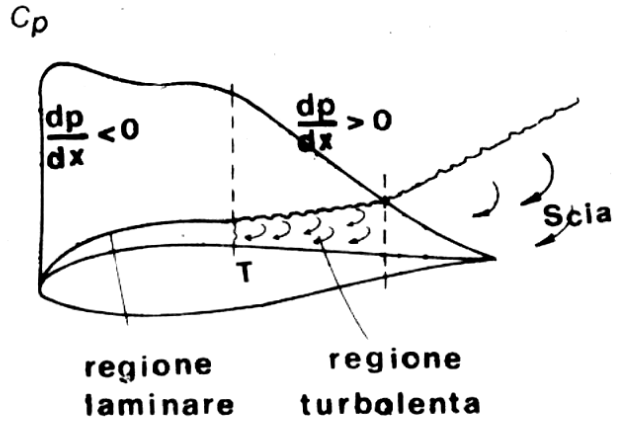

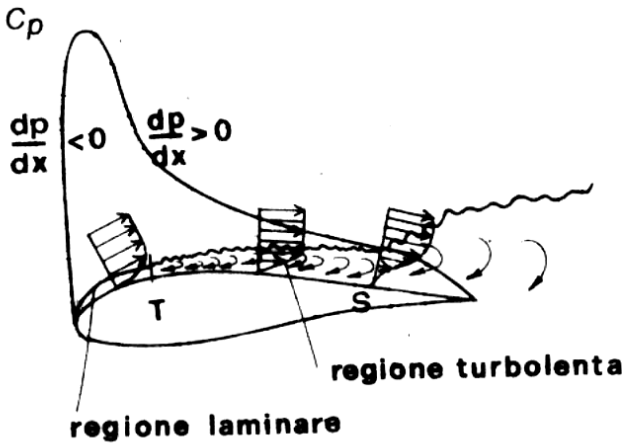

Lo strato limite è influenzata dalla distribuzione di pressione:

1. **Un Cp in espansione tende a favorire la presenza di fulsso laminare**
2. **Un Cp in compressione tende a favorire la transizione laminare-turbolenta**
3. **Un Cp in compressione tende a favorire le separazioni**

AERODINAMICA

RESISTENZA D'ATTRITO

Transizione dei flussi da laminari a turbolento
(riduzione del Reynolds critico)
Raffreddamento, suzione

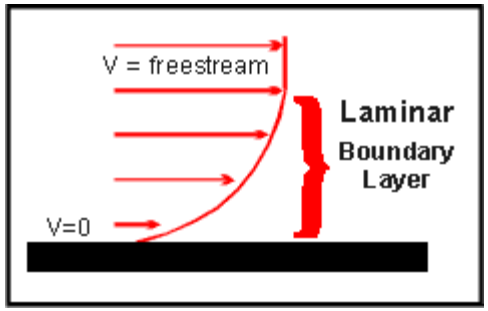

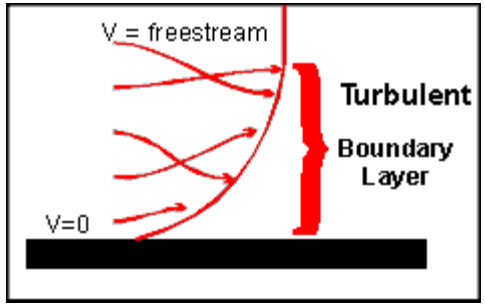

Riduzione degli sforzi di parete in flusso turbolento (Riblets, ….)
Circa 10 -15 %

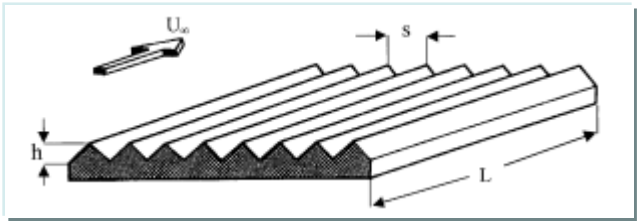

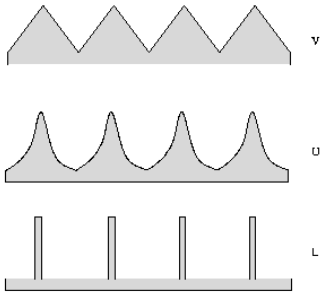

Stallo

Inclination Effects on Lift

Glenn Research Center

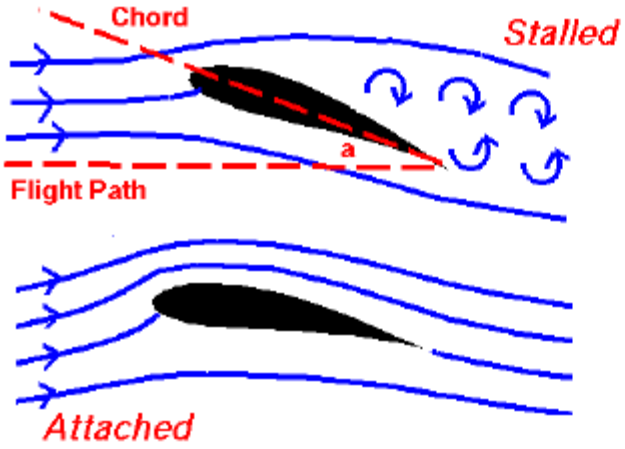

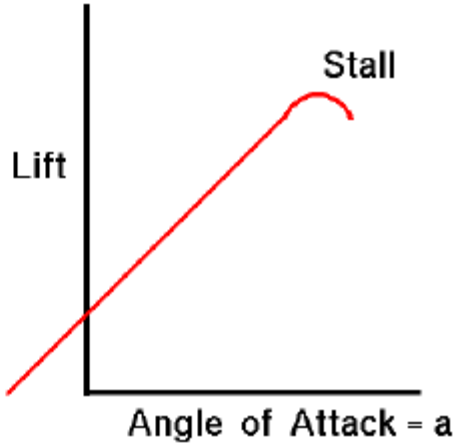

For small angles, lift is related to angle.

Greater Angle = Greater Lift

For larger angles, the lift relation is complex.

Included in Lift Coefficient

Il coefficiente di portanza è lineare all'aumentare dell'angolo d'attac
fino allo stallo quando comincia a diminuire in modo più o meno brus

Metodologie di analisi aerodinamica

$$\frac{\partial \rho}{\partial t} + \underline{\nabla} \cdot (\rho \underline{V}) = 0$$

$$\rho \left[\frac{\partial \underline{V}}{\partial t} + (\underline{V} \cdot \underline{\nabla}) \underline{V} \right] = -\underline{\nabla} P + \frac{1}{R_e} \underline{\nabla} \left[\lambda (\underline{\nabla} \cdot \underline{V}) \right] + \underline{\nabla} \cdot \left[\mu \left(\underline{\nabla V} + \underline{\nabla V}^{tr} \right) \right]$$

$$\rho \left[\frac{\partial T}{\partial t} + (\underline{V} \cdot \underline{\nabla}) T \right] - (\gamma - 1) M^2 \left[\frac{\partial P}{\partial t} + (\underline{V} \cdot \underline{\nabla}) P \right] =$$
$$\frac{1}{R_e} \underline{\nabla} \cdot (K \underline{\nabla} T) + \frac{(\gamma - 1) M^2}{R_e} \left\{ \lambda (\underline{\nabla} \cdot \underline{V})^2 + \frac{\mu}{2} \left[\underline{\nabla V} + \underline{\nabla V}^{tr} \right]^2 \right\}$$

$$P = \frac{\rho T}{\gamma M^2}$$

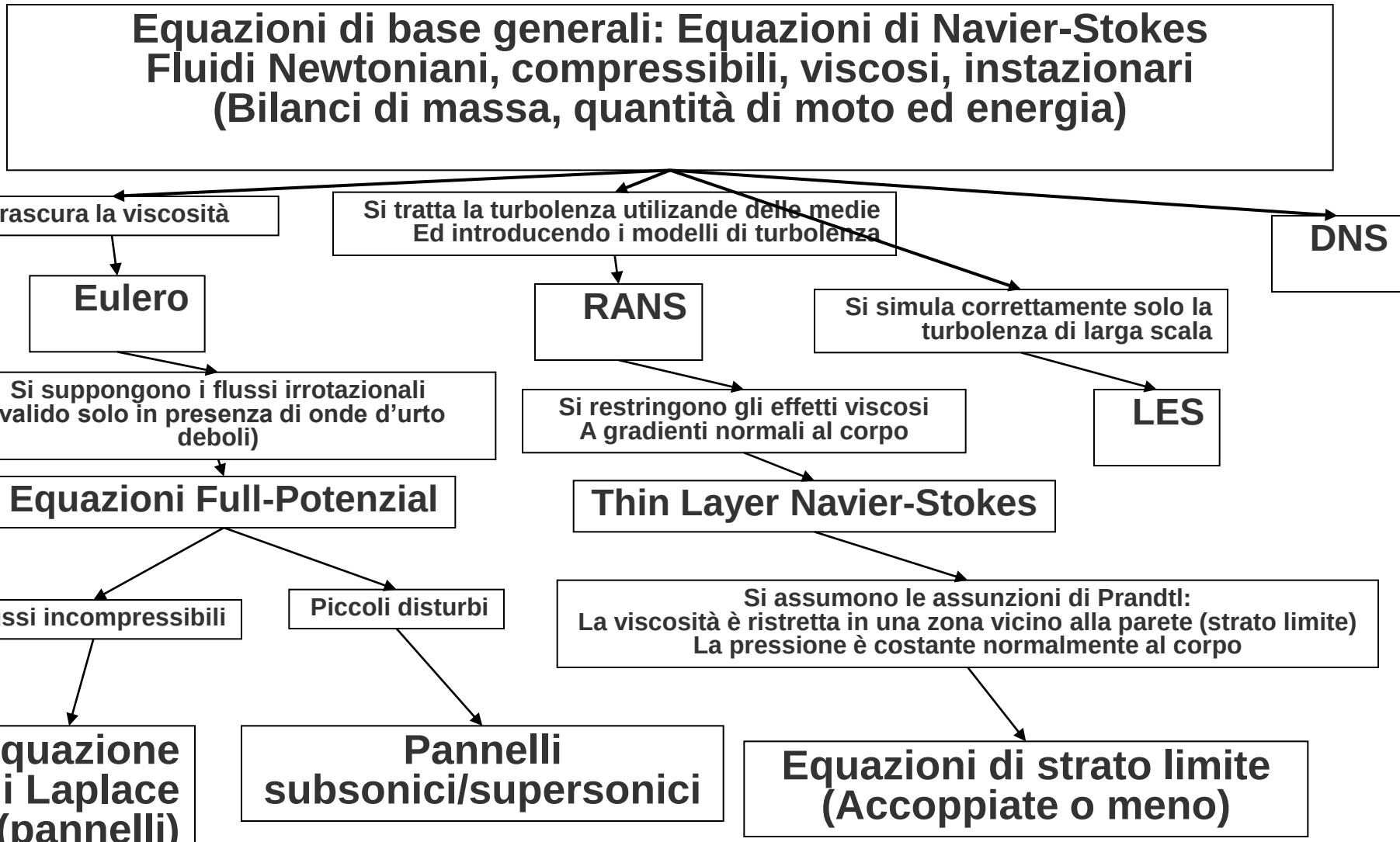

Metodi numerici: Pannelli

Linea portante

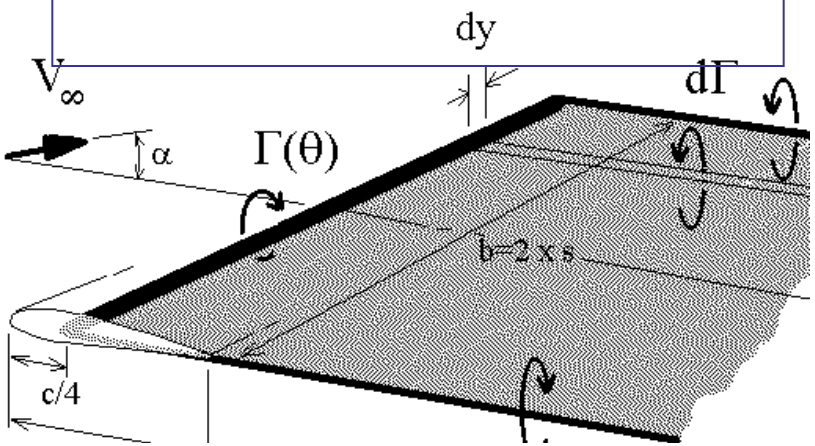

Vortex lattice

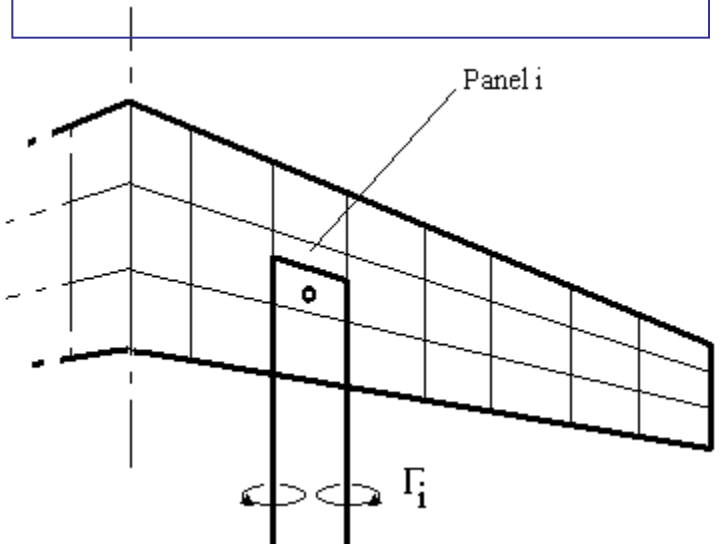

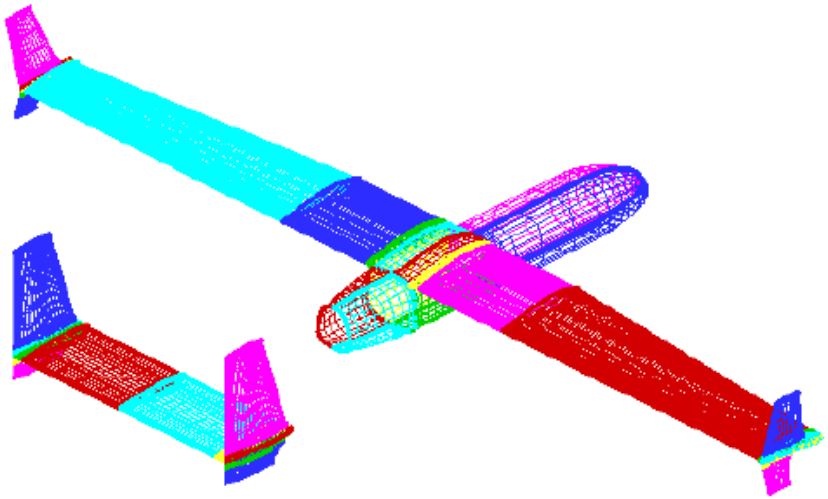

Pannelli superficiali

Metodi numerici: Pannelli

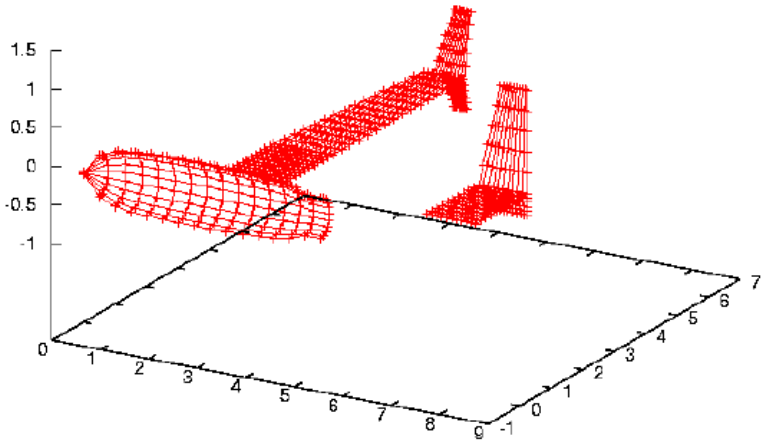

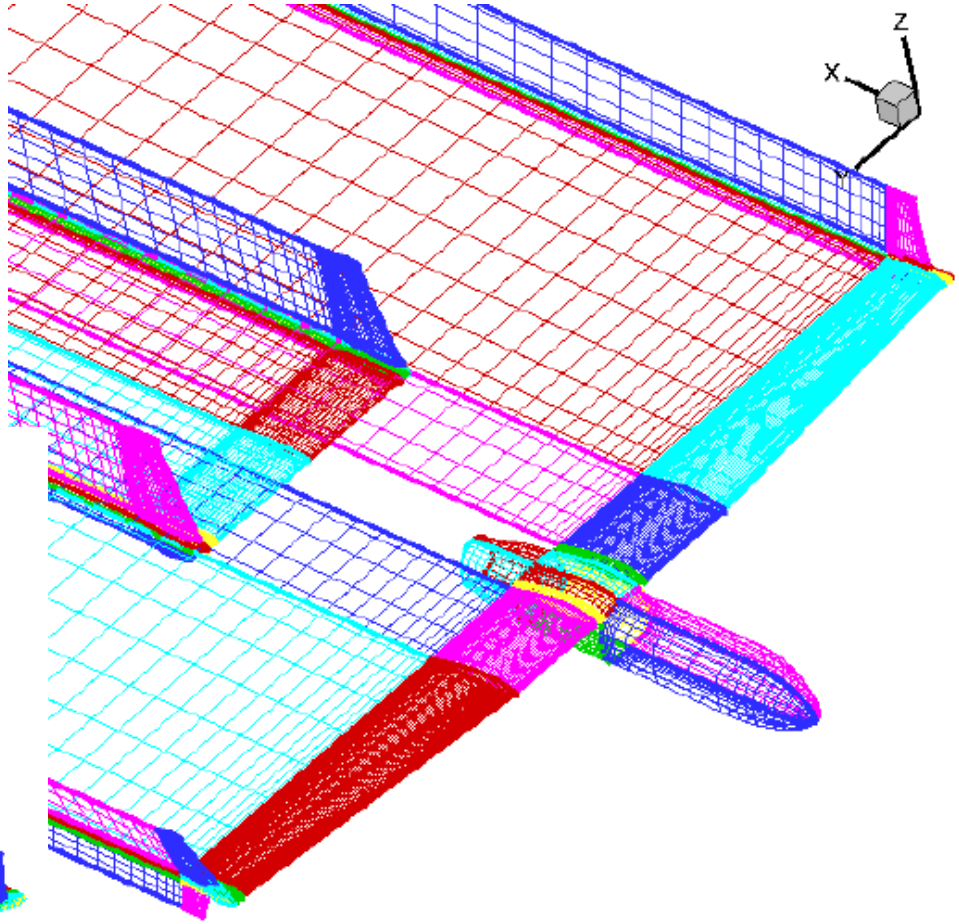

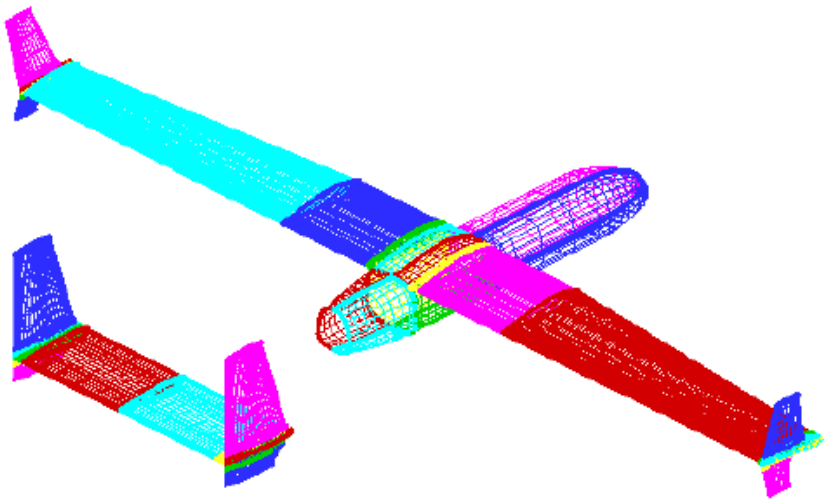

Metodi numerici: griglie Navier-Stokes

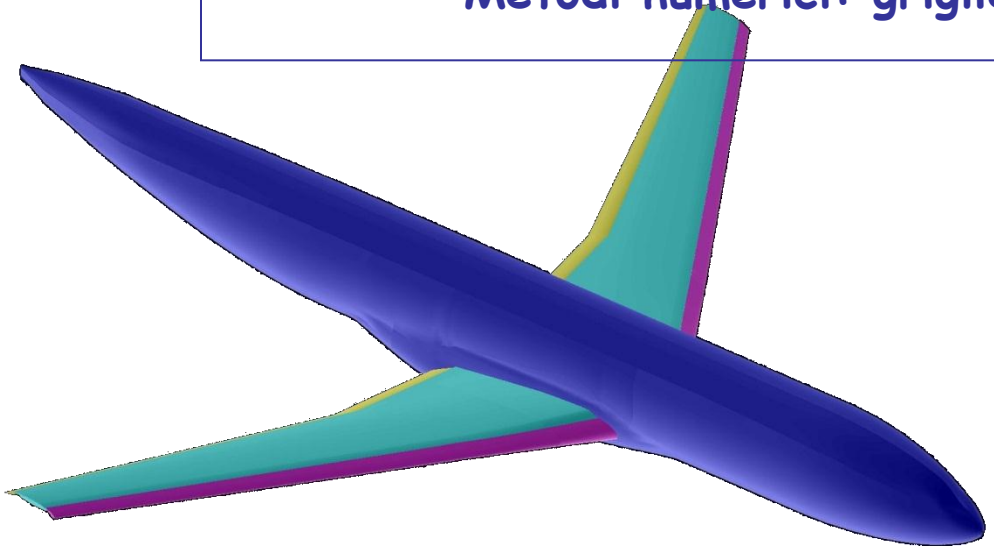

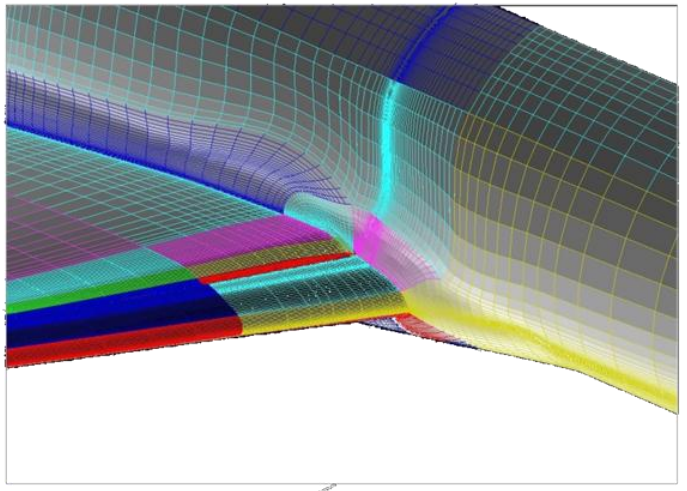

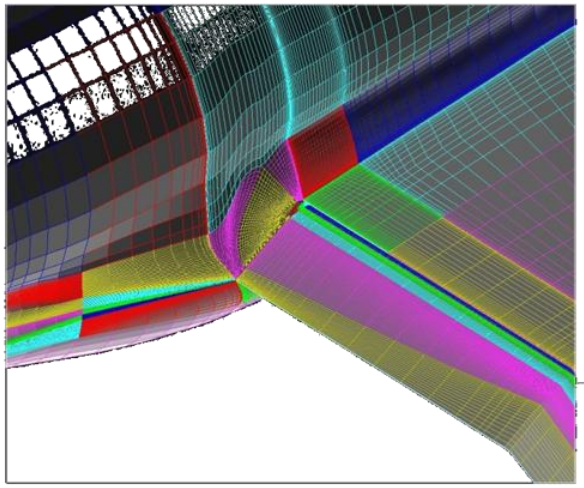

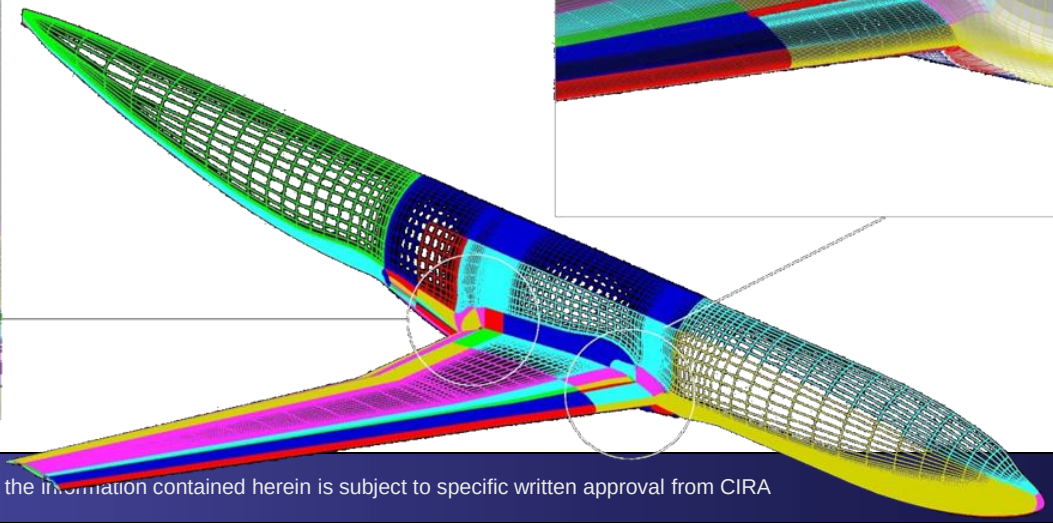

TRANSIZIONE LAMINARE TURBOLENTO

- Continuity

$$-\frac{\imath\gamma M^2 P}{T}(\alpha U+\beta V-\omega)\delta t_o+\imath\gamma M^2 P\alpha\delta u_o+\imath\gamma M^2 P\beta\delta v_o+\gamma M^2 P\frac{\partial\delta w_o}{\partial x_3}+$$
$$\gamma M^2\left[\frac{\partial P}{\partial x_3}-\frac{P}{T}\frac{\partial T}{\partial x_3}\right]\delta w_o+\imath\gamma M^2(\alpha U+\beta V-\omega)\delta p_o=0$$

- Momentum along η

$$\frac{1}{Re}\left\{-\mu\frac{\partial^2\delta v_o}{\partial x_3^2}-\frac{\partial V}{\partial x_3}\frac{\partial\mu}{\partial T}\frac{\partial\delta t_o}{\partial x_3}-\frac{\partial\mu}{\partial T}\frac{\partial T}{\partial x_3}\frac{\partial\delta v_o}{\partial x_3}-\imath\beta(\mu+\lambda)\frac{\partial\delta w_o}{\partial x_3}-\left(\frac{\partial\mu}{\partial T}\frac{\partial^2 V}{\partial x_3^2}+\frac{\partial V}{\partial x_3}\frac{\partial^2\mu}{\partial T^2}\frac{\partial T}{\partial x_3}\right)\delta t_o+\alpha\beta(\mu+\lambda)\delta u_o\right\}+$$
$$+\left\{\frac{\imath\gamma M^2 P}{T}(\alpha U+\beta V-\omega)+\frac{1}{Re}[\mu\alpha^2+\beta^2(\lambda+2\mu)]\right\}\delta v_o+\left(\frac{\gamma M^2 P}{T}\frac{\partial V}{\partial x_3}-\frac{\imath\beta}{Re}\frac{\partial\mu}{\partial T}\frac{\partial T}{\partial x_3}\right)\delta w_o+\imath\beta\delta p_o=0$$

- Momentum along x_3

$$\frac{1}{Re}\left\{-(\lambda+2\mu)\frac{\partial^2\delta w_o}{\partial x_3^2}-\imath\alpha(\mu+\lambda)\frac{\partial\delta u_o}{\partial x_3}-\imath\beta(\mu+\lambda)\frac{\partial\delta v_o}{\partial x_3}-\frac{\partial T}{\partial x_3}\left(2\frac{\partial\mu}{\partial T}+\frac{\partial\lambda}{\partial T}\right)\frac{\partial\delta w_o}{\partial x_3}-\imath\frac{\partial\mu}{\partial T}\left(\alpha\frac{\partial U}{\partial x_3}+\beta\frac{\partial V}{\partial x_3}\right)\delta t_o\right\}+$$
$$+\frac{\partial\delta p_o}{\partial x_3}-\frac{\imath\alpha}{Re}\frac{\partial\lambda}{\partial T}\frac{\partial T}{\partial x_3}\delta u_o-\frac{\imath\beta}{Re}\frac{\partial\lambda}{\partial T}\frac{\partial T}{\partial x_3}\delta v_o+\left[\frac{\imath\alpha M^2 P}{T}(\alpha U+\beta V-\omega)+\frac{\mu}{Re}(\alpha^2+\beta^2)\right]\delta w_o=0$$

- Momentum along ξ

$$\frac{1}{Re}\left\{-\mu\frac{\partial^2\delta u_o}{\partial {x_3}^2}-\frac{\partial U}{\partial x_3}\frac{\partial\mu}{\partial T}\frac{\partial\delta t_o}{\partial x_3}-\frac{\partial T}{\partial x_3}\frac{\partial\mu}{\partial T}\frac{\partial\delta u_o}{\partial x_3}-\imath\alpha(\mu+\lambda)\frac{\partial\delta w_o}{\partial x_3}-\left[\frac{\partial U}{\partial x_3}\frac{\partial T}{\partial x_3}\frac{\partial^2\mu}{\partial T^2}+\frac{\partial^2 U}{\partial {x_3}^2}\frac{\partial\mu}{\partial T}\right]\delta t_o\right\}+\left[\imath\frac{\gamma M^2 P}{T}\right.$$
$$\left.(\alpha U+\beta V-\omega)+\frac{1}{Re}\left((2\mu+\lambda)\alpha^2+\mu\beta^2\right)\right]\delta u_o+\frac{\beta\alpha}{Re}(\mu+\lambda)\delta v_o+\left[\frac{\gamma M^2 P}{T}\frac{\partial U}{\partial x_3}-\frac{\imath\alpha}{Re}\frac{\partial\mu}{\partial T}\frac{\partial T}{\partial x_3}\right]\delta w_o+\imath\alpha\delta p_o=0$$

TRANSIZIONE LAMINARE TURBOLENTO

- Energy

$$-\frac{K}{Re}\frac{\partial^2 \delta t_o}{\partial x_3^2}+\left\{\frac{\imath\gamma M^2 P}{T}(\alpha U+\beta V-\omega)+\frac{K}{Re}(\alpha^2+\beta^2)-(\gamma-1)\frac{M^2}{Re}\frac{\partial \mu}{\partial T}\left[\left(\frac{\partial U}{\partial x_3}\right)^2+\left(\frac{\partial V}{\partial x_3}\right)^2\right]-\frac{1}{Re}\left[\frac{\partial^2 K}{\partial T^2}\left(\frac{\partial T}{\partial x_3}\right)^2+\right.\right.$$

$$\left.\left.+\frac{\partial^2 T}{\partial x_3^2}\left(\frac{\partial K}{\partial T}\right)\right]\right\}\delta t_o-(\gamma-1)M^2\imath(\alpha U+\beta V-\omega)\delta p_o-2(\gamma-1)\frac{M^2\mu}{Re}\frac{\partial U}{\partial x_3}\frac{\partial \delta u_o}{\partial x_3}+\left[-2(\gamma-1)M^2\frac{\imath}{Re}\mu\beta\frac{\partial V}{\partial x_3}+\right.$$

$$\left.-(\gamma-1)M^2\frac{\partial P}{\partial x_3}-(\gamma-1)\frac{2M^2\imath\alpha}{Re}\mu\frac{\partial U}{\partial x_3}+\frac{\gamma M^2 P}{T}\frac{\partial T}{\partial x_3}\right]\delta w_o-2(\gamma-1)\frac{M^2\mu}{Re}\frac{\partial V}{\partial x_3}\frac{\partial \delta v_o}{\partial x_3}-\frac{2}{Re}\frac{\partial K}{\partial T}\frac{\partial T}{\partial x_3}\frac{\partial \delta t_o}{\partial x_3}=0$$

Basso Reynolds e Basso Mach

Transoniche (CIRA-PT1)

Subsoniche CIRA (IWT)

LAMINAR FLOW TECHNOLOGY:

Hybrid Laminar Flow Control (9% reduction in fuel saving)

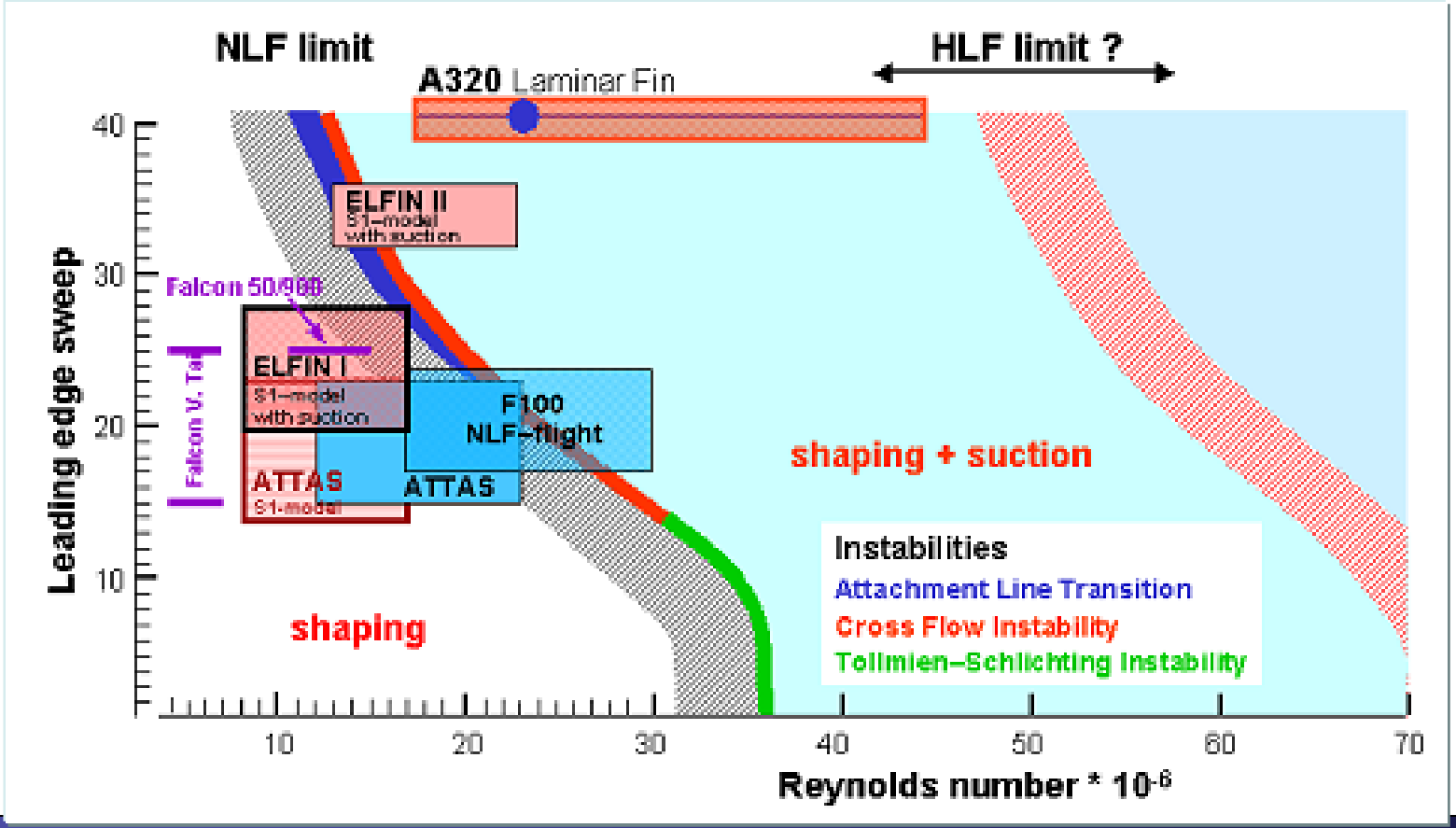

LAMINAR FLOW TECHNOLOGY:

Hybrid Laminar Flow Control (9% reduction in fuel saving)

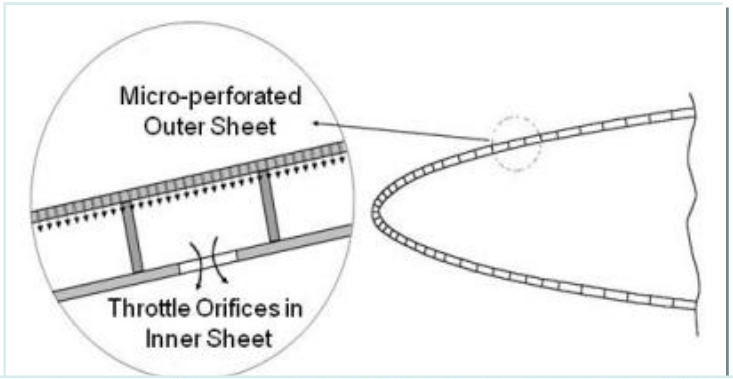

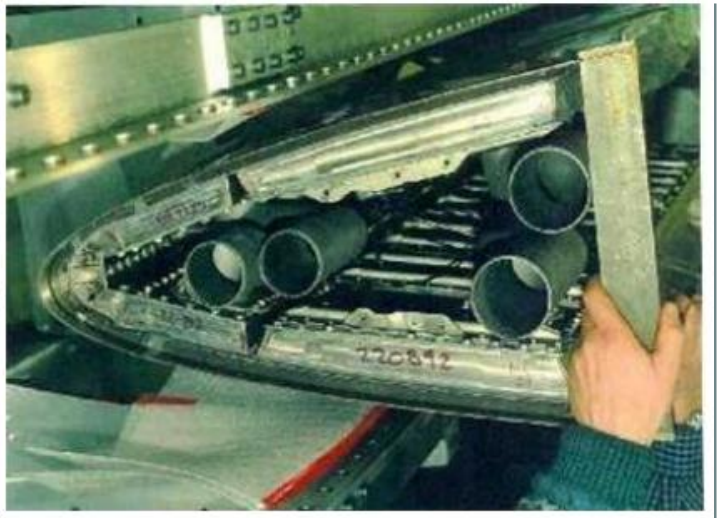

Automatic 3D flap shape-modification/positioning & droop spoiler rotation

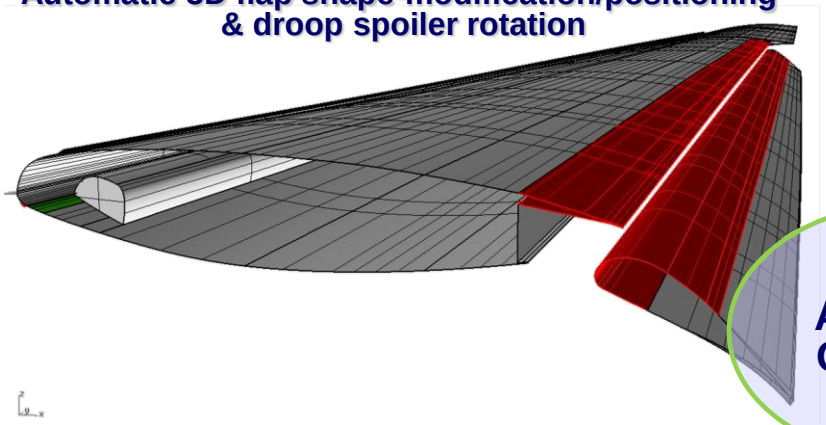

Automatic 3D Krueger shape-modification/positioning

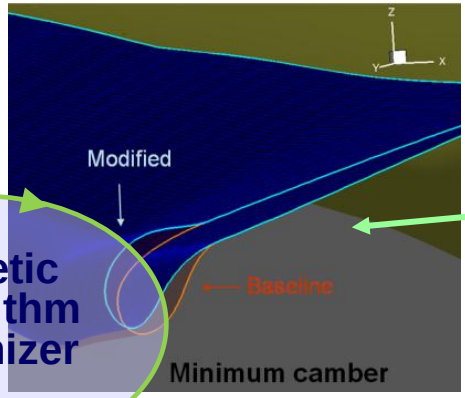

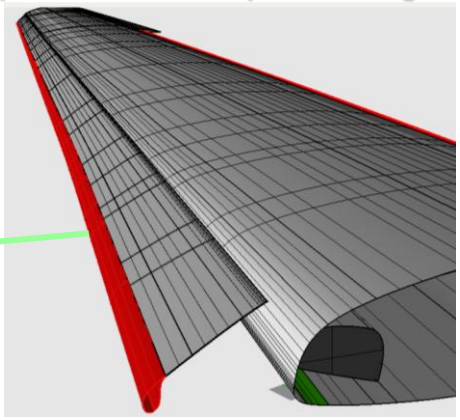

Genetic Algorithm Optimizer

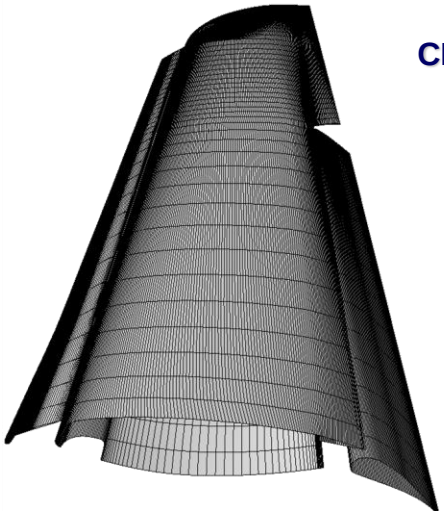

Parametric CFD mesh (4 Mcells)

CFD Analysis of initial configuration (flap separation)

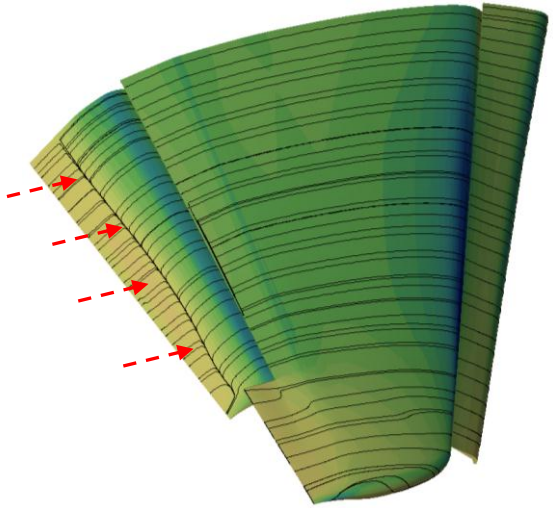

Minimized flap separation after some steps of optimization

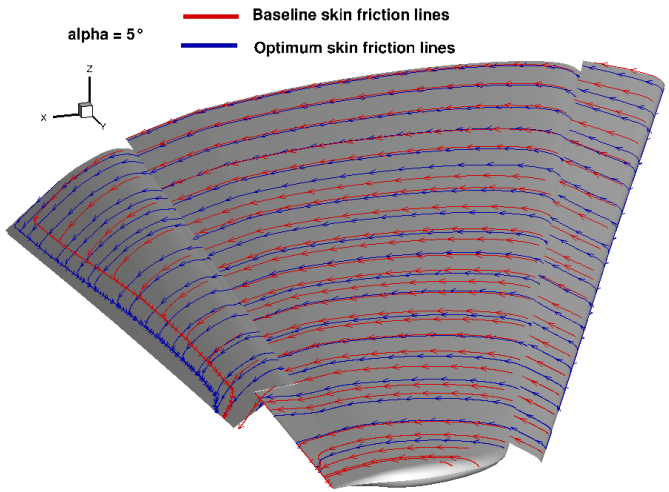

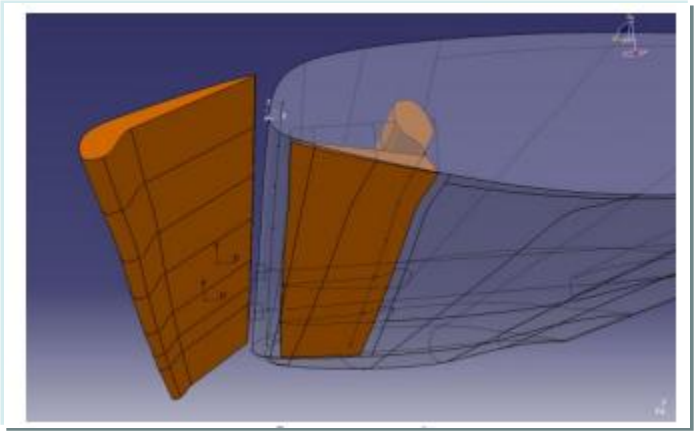

- **INTEGRAZIONE DEL SISTEMA DI PROTEZIONE DAL GHIACCIO CON IL SISTEMA DI SUZIONE**

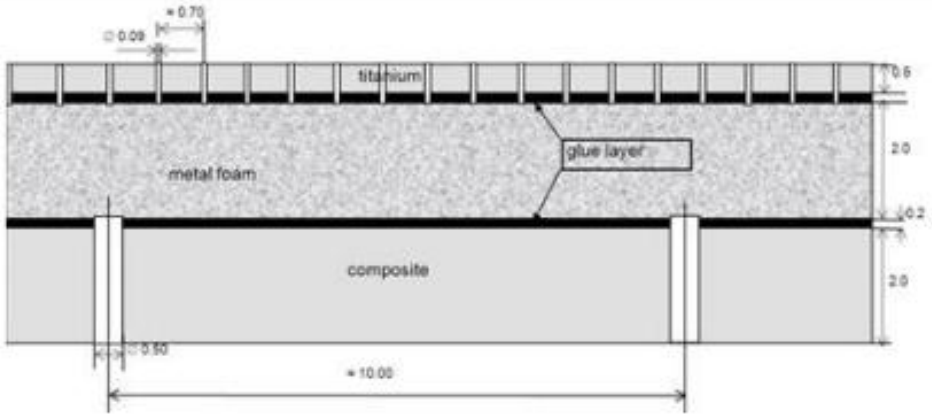

Figure 41: Combined Fibre Metal Laminate skin of FOKK (left), skin concept of NLR (right)

- **AFC technologies for local flow separation control applied in wing/pylon junction to improve performances and load situation mainly in landing conditions. The technologies are crucial for the integration of Ultra High Bypass Ratio to balance a loss of 5% maximum lift**

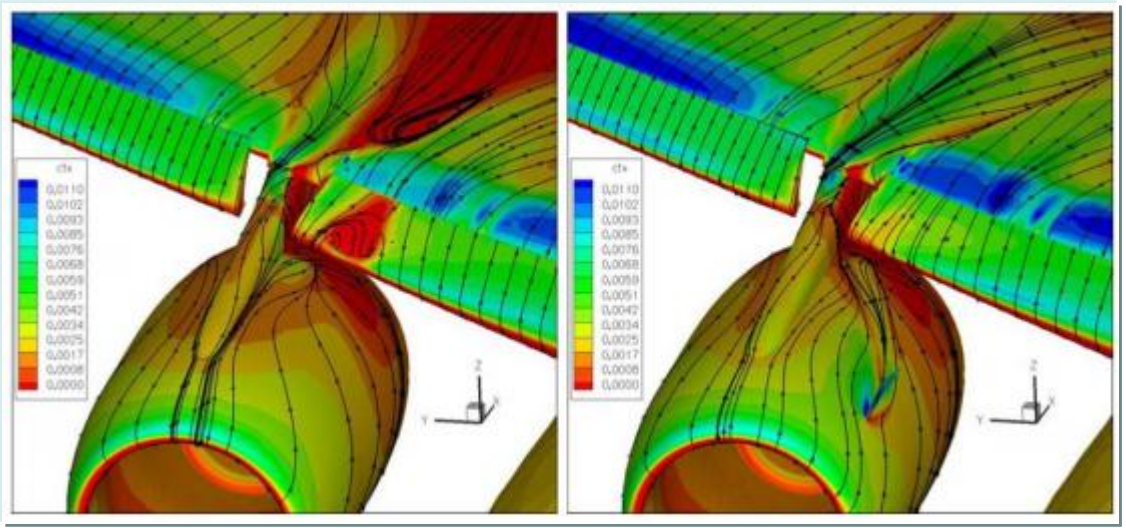

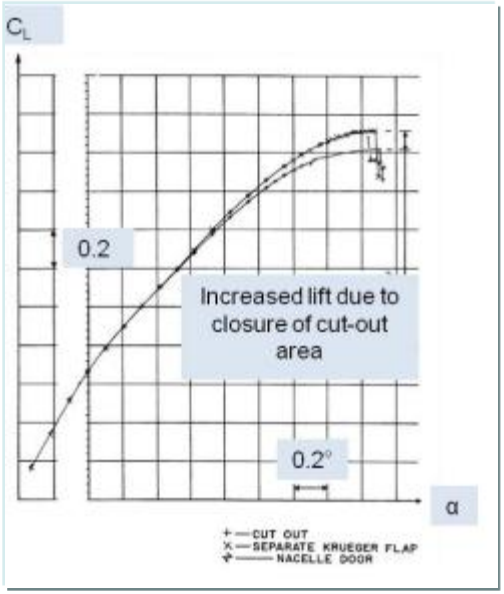

- **WHY to control the flow???**

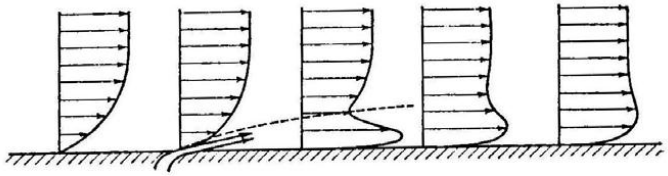

HOW???

- **Prevent separation of the flow**
- **Modify the laminar-turbulent transition**
- **Enhance the lift of airfoils**
- **Reduce the drag**
- **Reduce unsteadiness**

Passive Flow Control

Active Flow Control…Plasma Actuators

- **Open loop**
- **Closed loop**

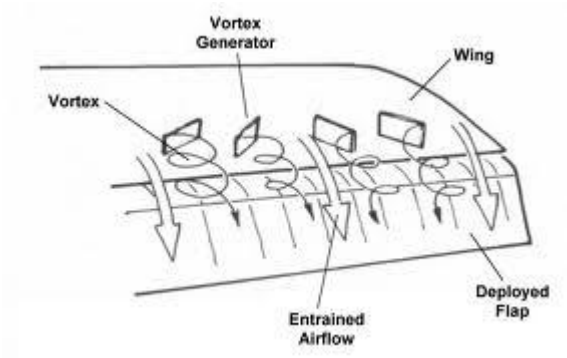

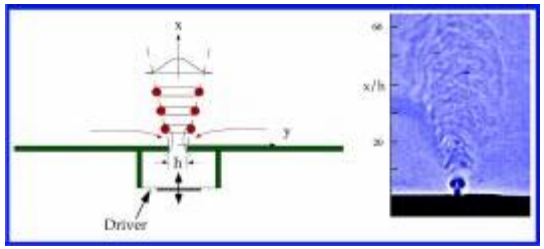

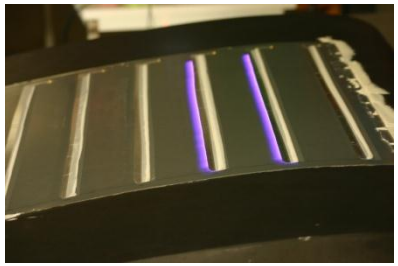

First Concept (DBD)

Surface Discharge actuators as "Dielectric Barrier Discharge (DBD)" whereby plasma is generated by the application of a high-voltage discharge between two electrodes which creates an ionization field and amongst the outcomes, a corresponding ionic wind due to the movement of ions at the surface of the airfoil very close to the wall.

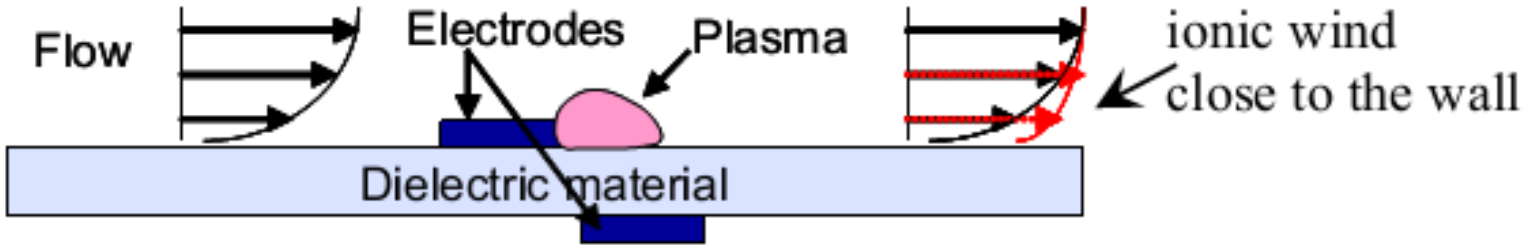

Second Concept (PSJ)

Spark plasma actuators known as "Plasma Synthetic Jet" (PSJ) where a plasma arc positioned inside a micro-cavity containing a small orifice adjacent to the airfoil's surface, causes an electro-thermally heating of the gas inside which leads to a rapid increase in pressure.

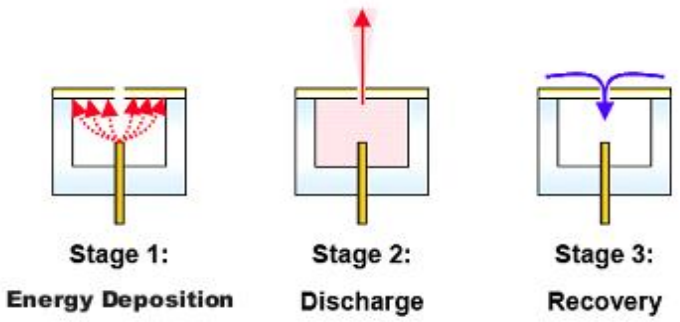

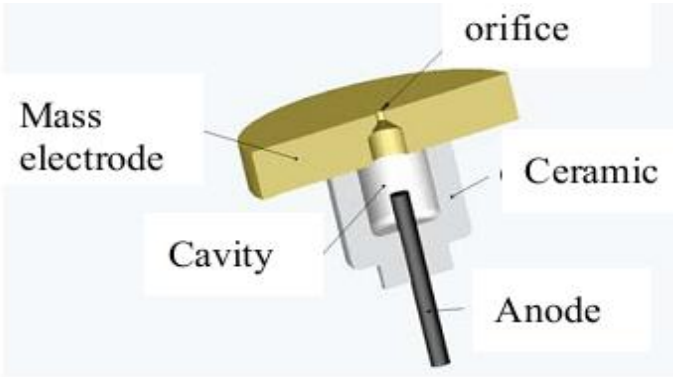

- **Plasma actuator for flow control can be used for:**

✓ **Separation control: high lift improvements**

✓ **Laminar/turbulent transition control**

✓ **Shock separation control/Buffeting control**

✓ **Acoustic noise reduction**

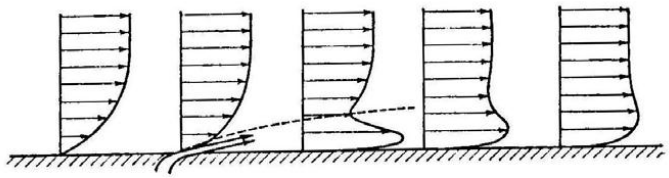

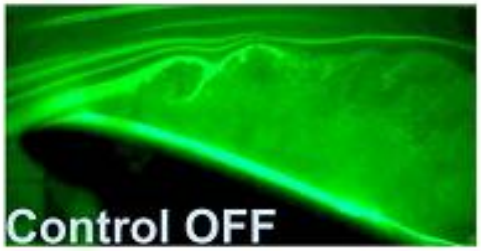

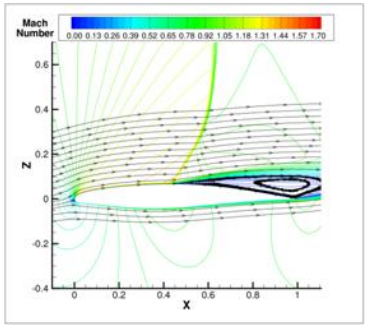

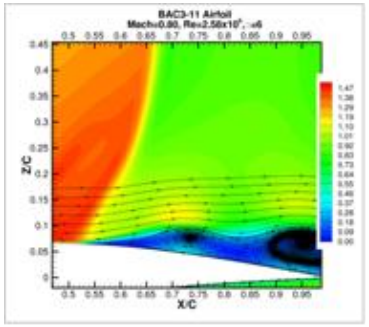

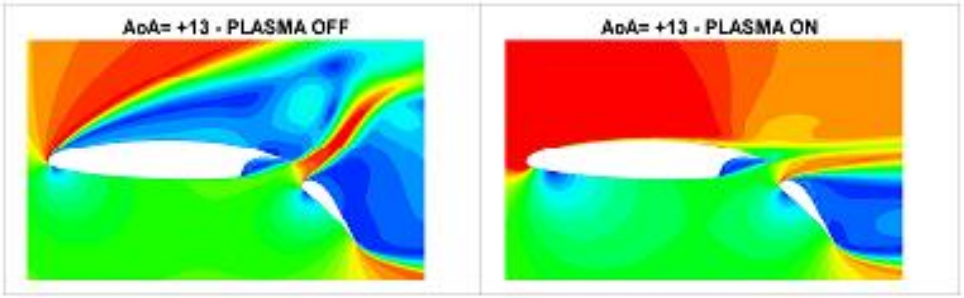

CON L'INTRODUZIONE DI NOTORI HBR PER RIDURRE IL CONSUMO DI COMBUSTIBILE l'AIRFRAME NOISE DIVENTA PREVALENTE RISPETTO AL RUMORE DEL MOTORE

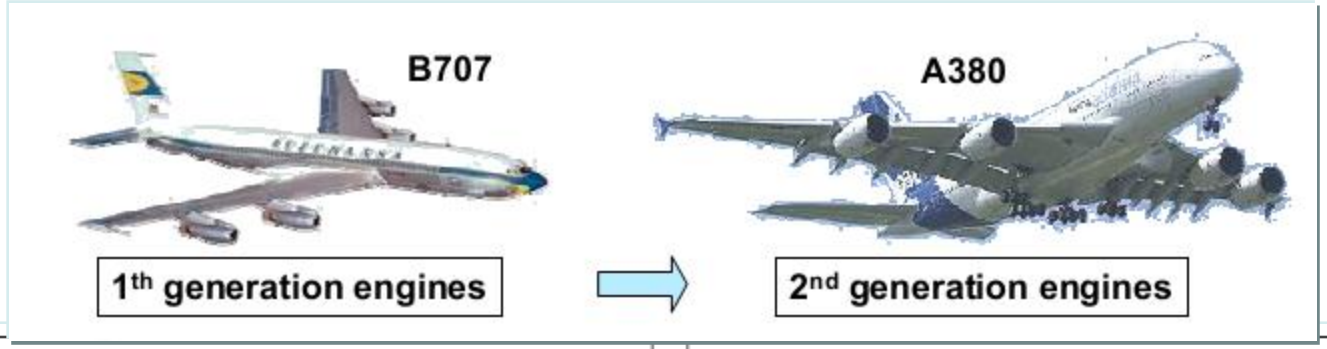

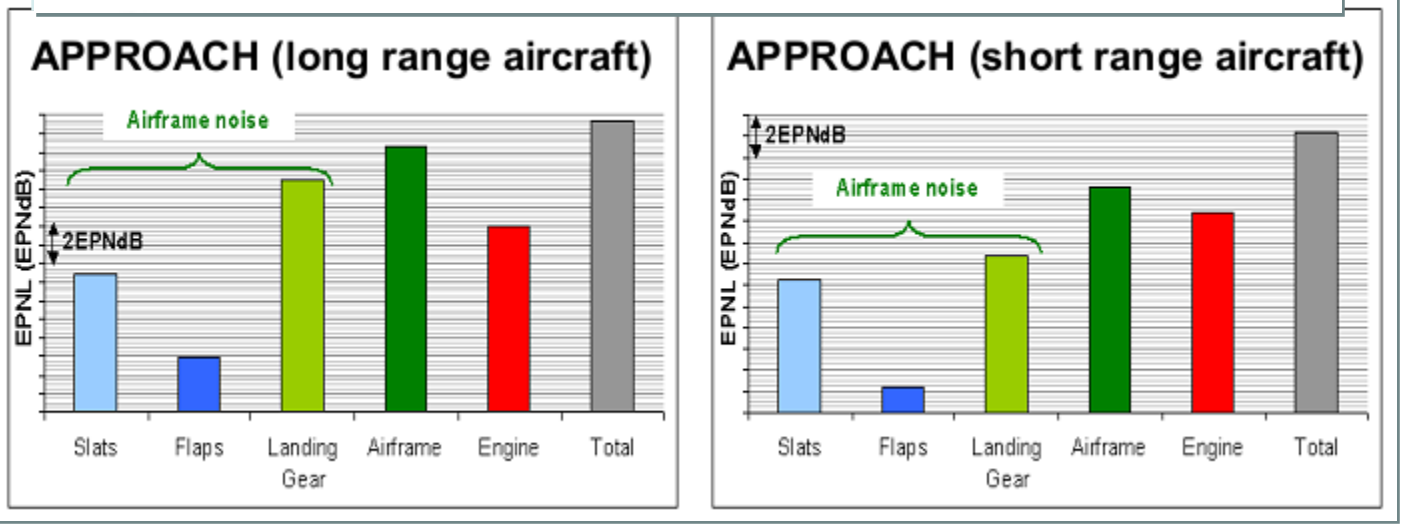

CON L'INTRODUZIONE DI NOTORI HBR PER RIDURRE IL CONSUMO DI COMBUSTIBILE l'AIRFRAME NOISE DIVENTA PREVALENTE RISPETTO AL RUMORE DEL MOTORE

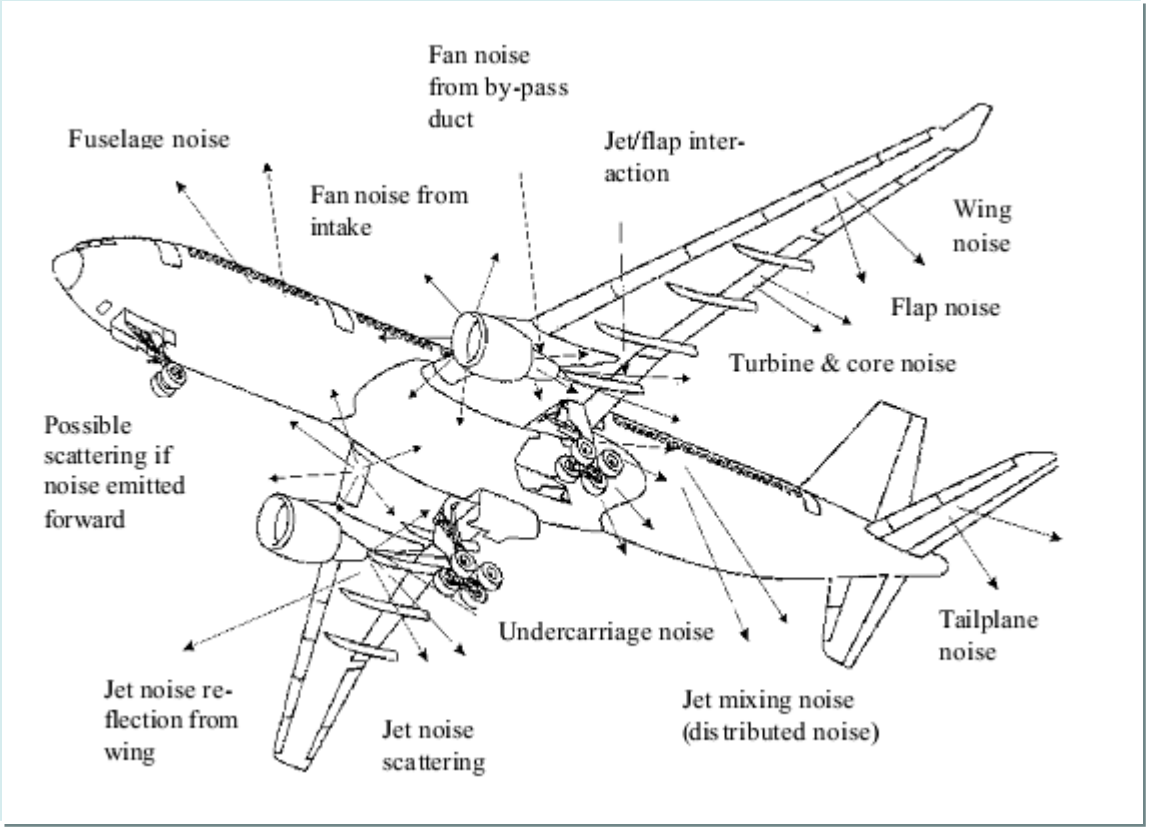

- **FLAP SIDE EDGE NOISE**

CIRA performed CFD/CAA and wind tunnel tests to reduce flap side edge noise by using side-fences

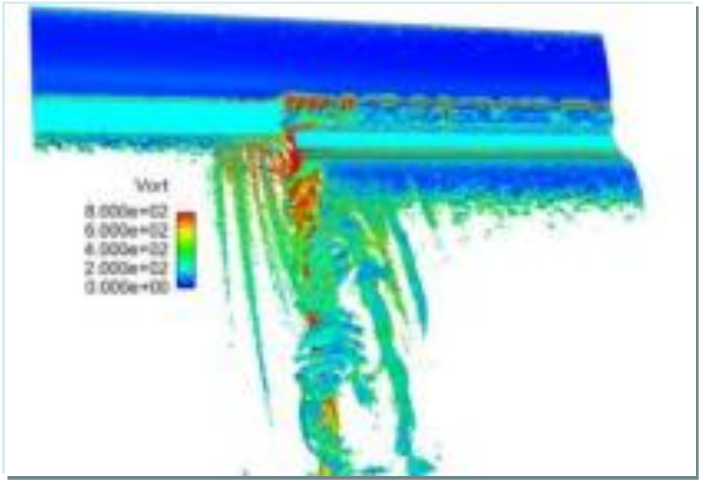

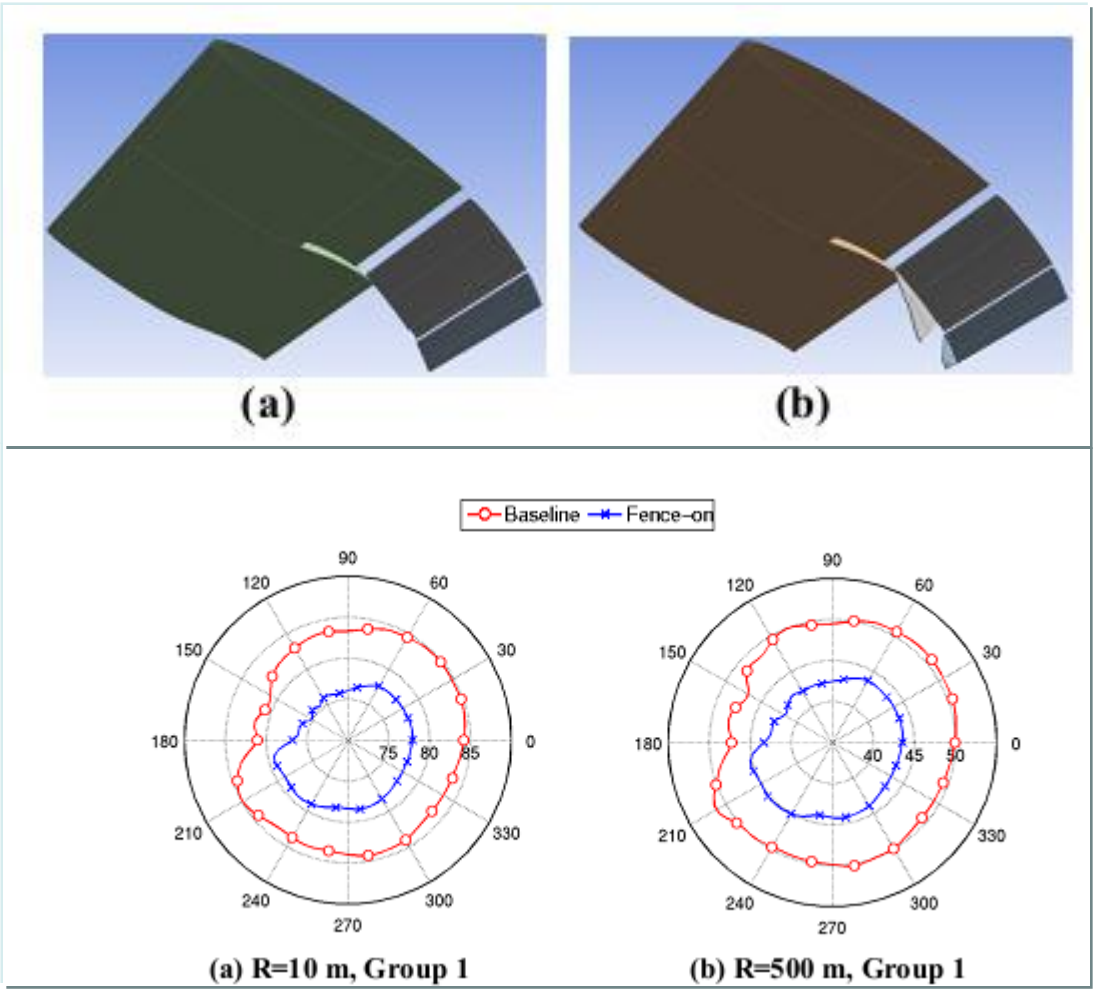

- **FLAP SIDE EDGE NOISE**

CIRA performed CFD/CAA and wind tunnel tests to reduce flap side edge noise by using side-fences

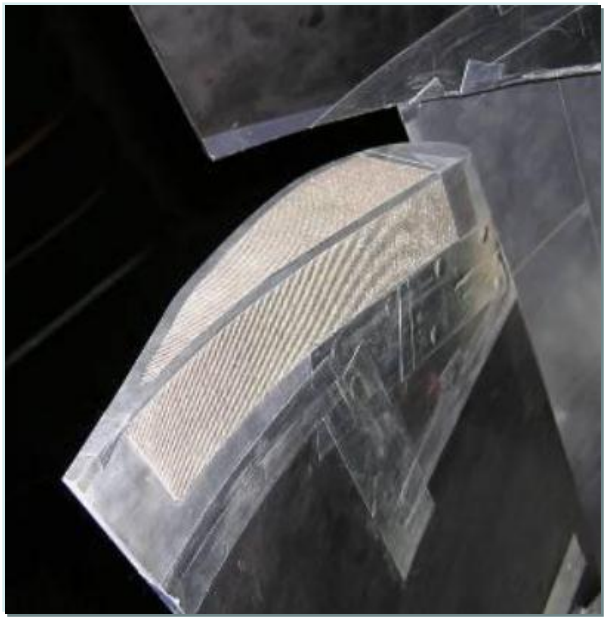

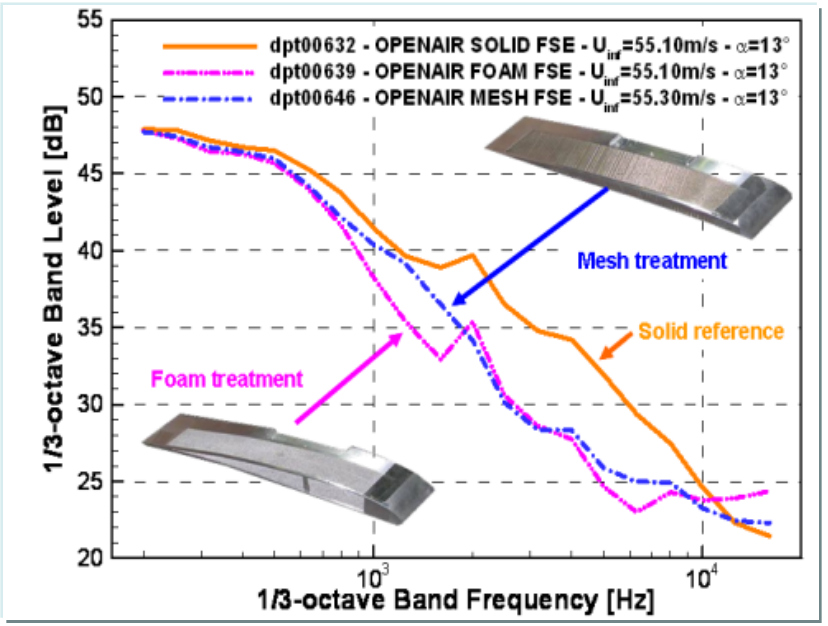

- **LANDING GEAR NOISE**

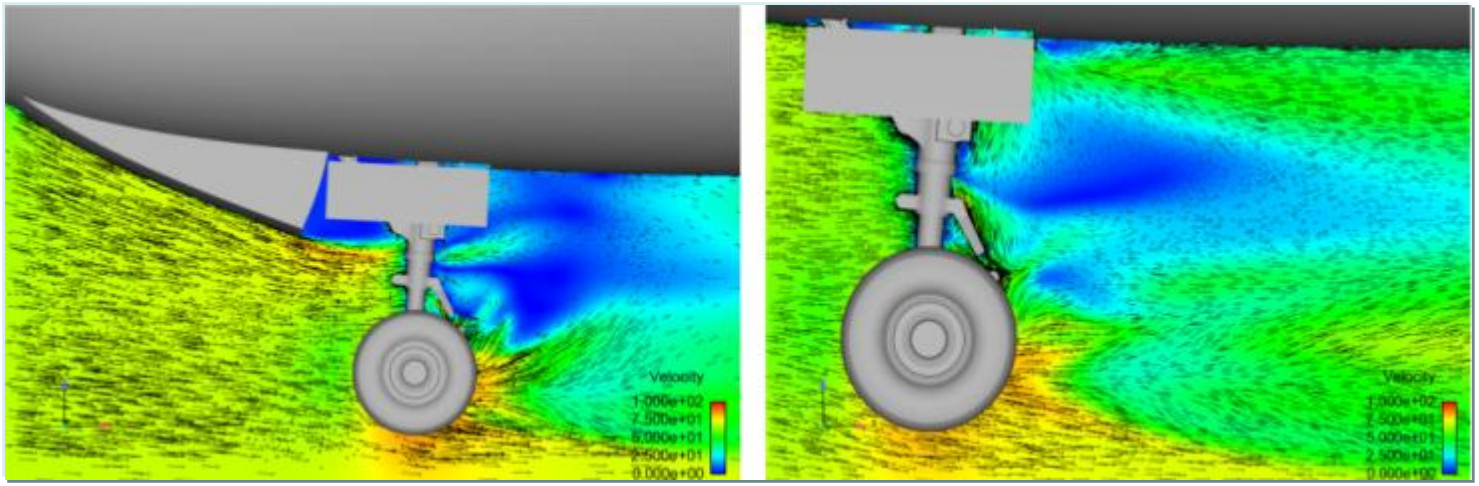

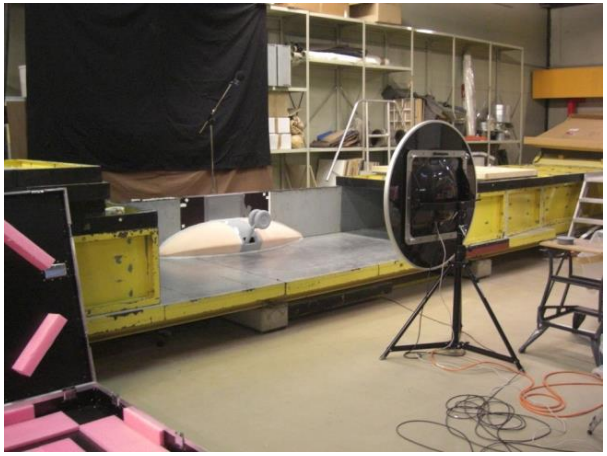

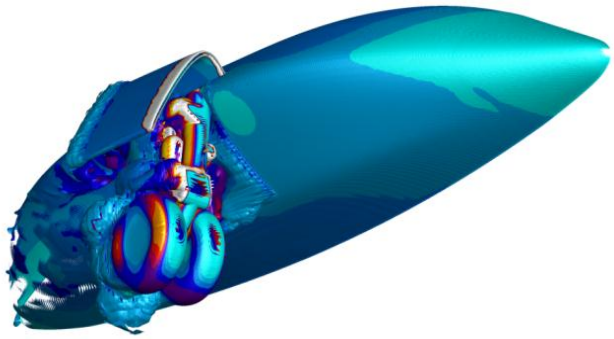

#MLG1: *leg fairing*

(0 – 2 dB) estimated noise reduction

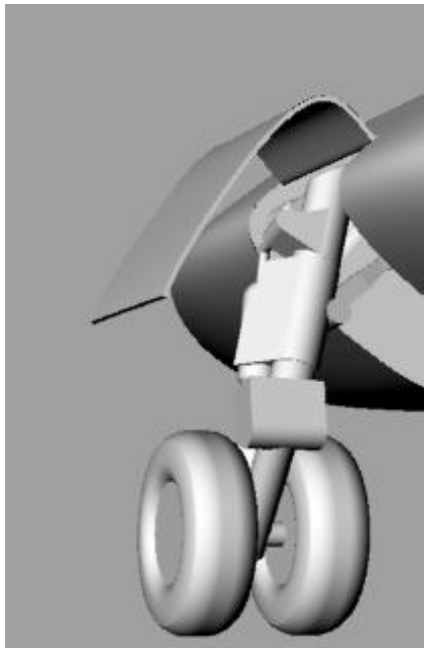

#MLG2: *leg fairing*

(0 dB) estimated noise reduction

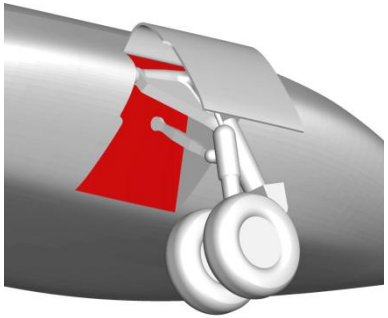

#MLG3: *bay liners*

(1.8 dB) estimated noise reduction

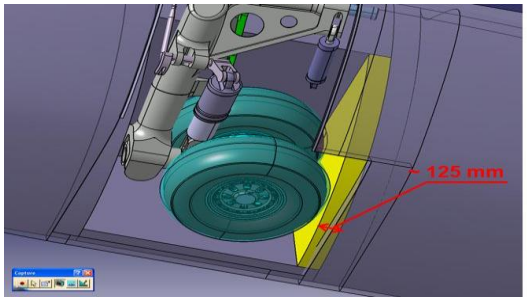

#MLG4: *perforated fairings*

(2 -4 dB) estimated noise reduction

#MLG5: *bay absorber*

(1 -2 dB) estimated noise reduction

#MLG6: *perforated fairings*

(1.8 dB) estimated noise reduction

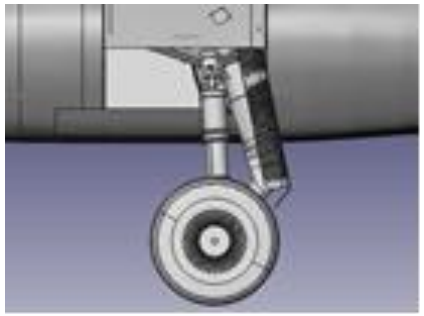

#MLG7: *meshes*

(2.4dB) estimated noise reduction

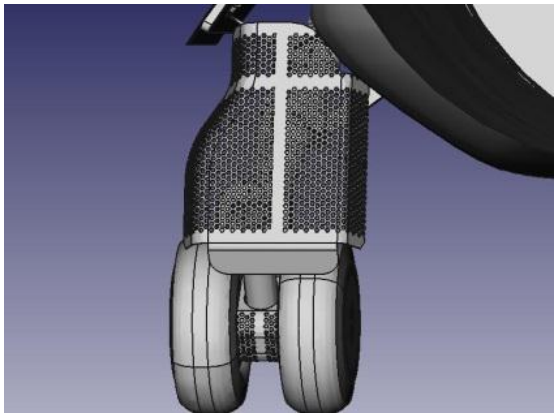

#MLG10: *sliding doors*

(1 -2 dB) estimated noise reduction

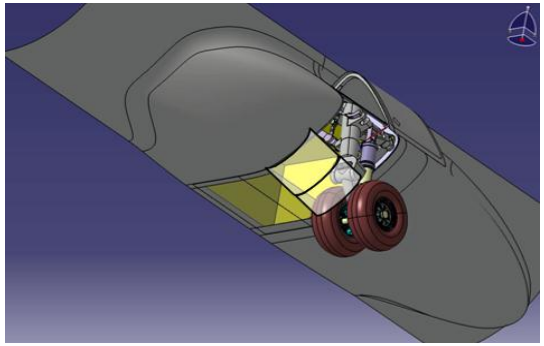

#MLG12: *spoiler*

(2 -4 dB) estimated noise reduction

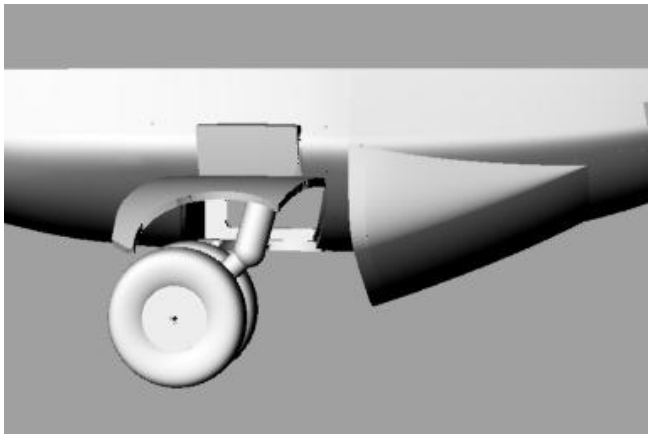

#MLG8: *wheel hub and cap*

(0.94 dB) estimated noise reduction

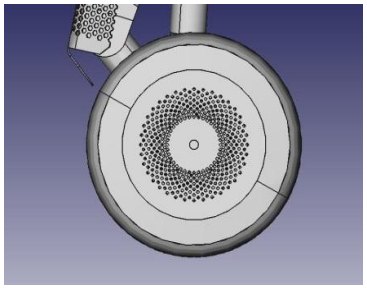

✓ 2 Baseline Engine – ***Turbo Prop 100*** : P=180 kW with constant-speed propeller
Unmanned Aerial Vehicles (*UAVs*) and Unmanned Combat Aerial Veichles (UCAVs)

STUDIO INSTALLAZIONE MOTORE EM-11C ORKCA

EM-11C ORKA, all composite light, twin airplane

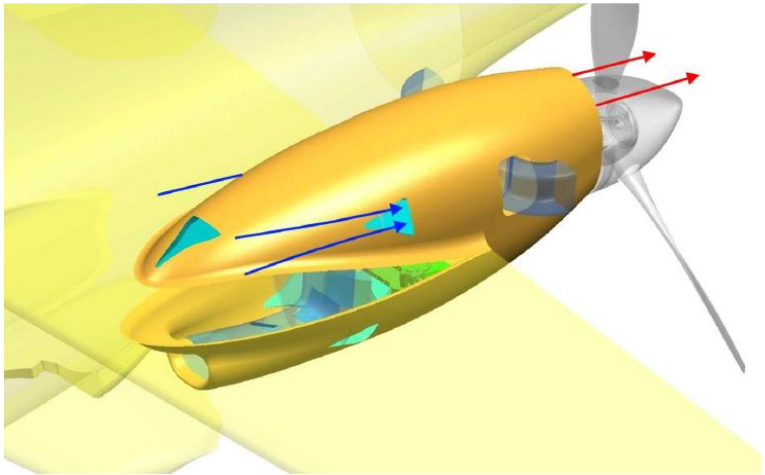

Engine Nacelle ventilation

Challenges:

- **Efficienza della presa d'aria;**
- **Volo in condizioni di formazione ghiaccio;**
- **Riscaldamento aerodinamico.**

Feature	
Maximum speed	359 km/h (194 kts)
Cruise speed	261 km/h (141 kts)
Stall speed	109 km/h (59 kts)
Range	1700 km (918 nm)
Rate of climb	5,1 m/s (1000 ft/min)

Feature	
Crew	One pilot
Capacity	3 passengers
Length	8.705 m (28.56 ft)
Wingspan	13.5 m / 10.5 folded wing tips (44.3 ft / 34.4 ft folded wing tips)
Height	5.585 m (8.48 ft)
Wing area	16.5 m² (177.61 sq. ft)
Useful load	550kg (1,212.5 lbs)
Max. takeoff weight	1,820 kg (4,012 lbs)
Powerplant	2xLycoming IO-320 air-cooled inline engine, 118 kW (160PS) each

Gennaro Serino
(g.serino@cira.it)

DISEGNO AERODINAMICO PRESA D'ARIA

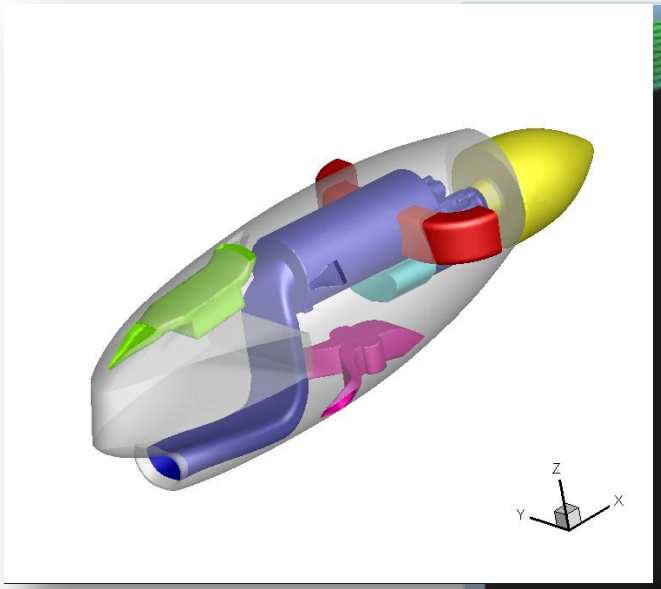

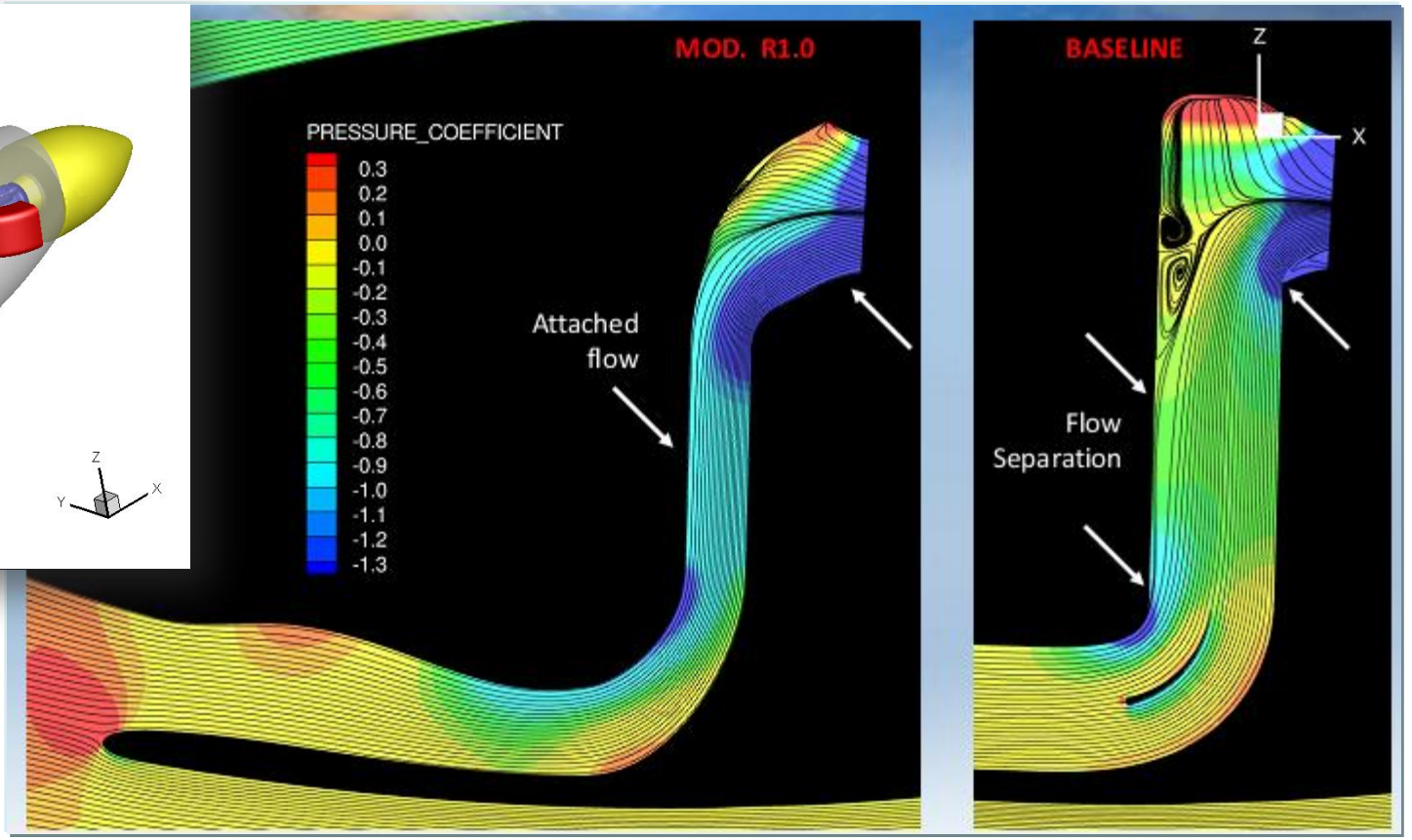

Gennaro Serino
(g.serino@cira.it)

DISEGNO AERODINAMICO PRESA D'ARIA

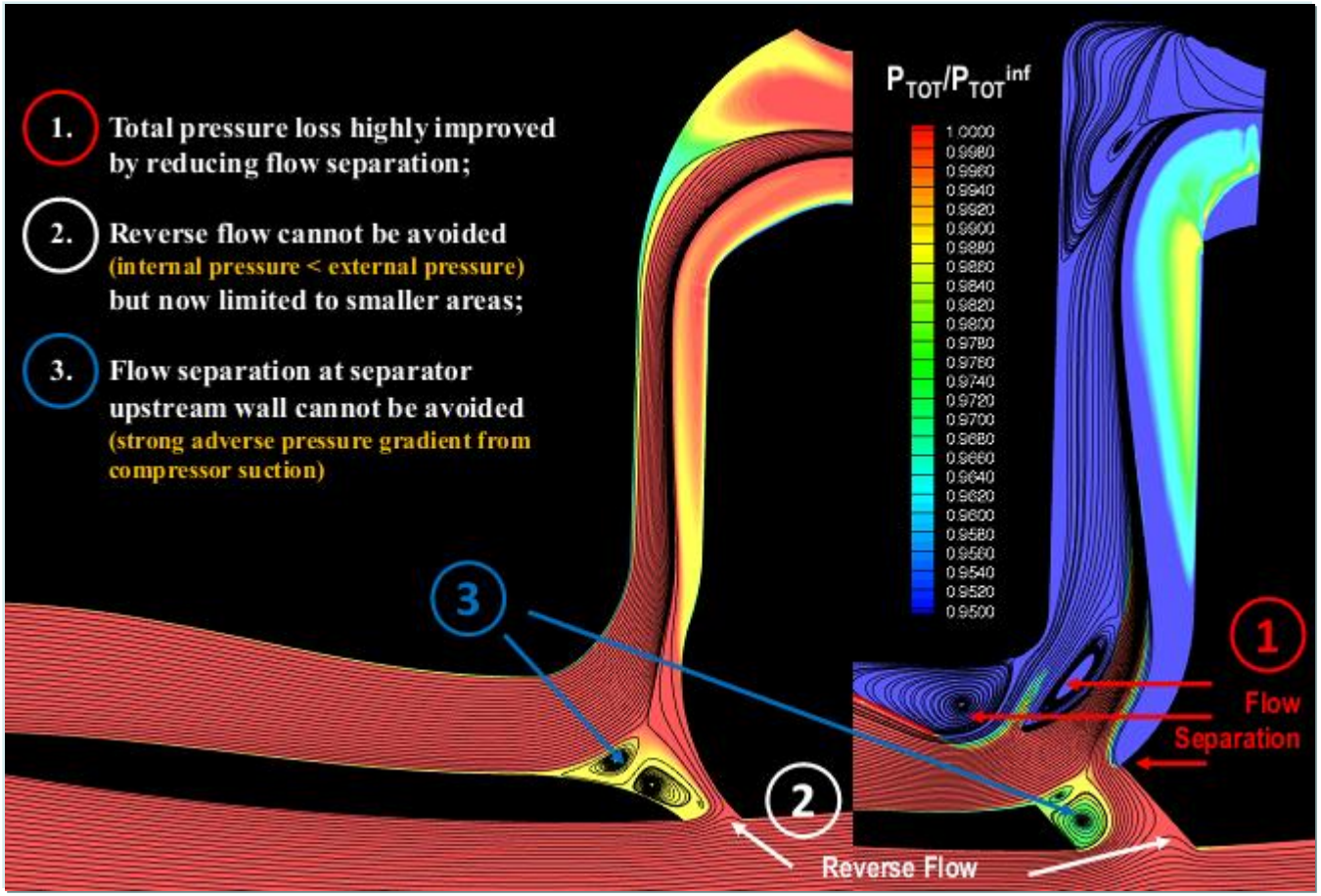

Gennaro Serino
(g.serino@cira.it)

(20 microns)

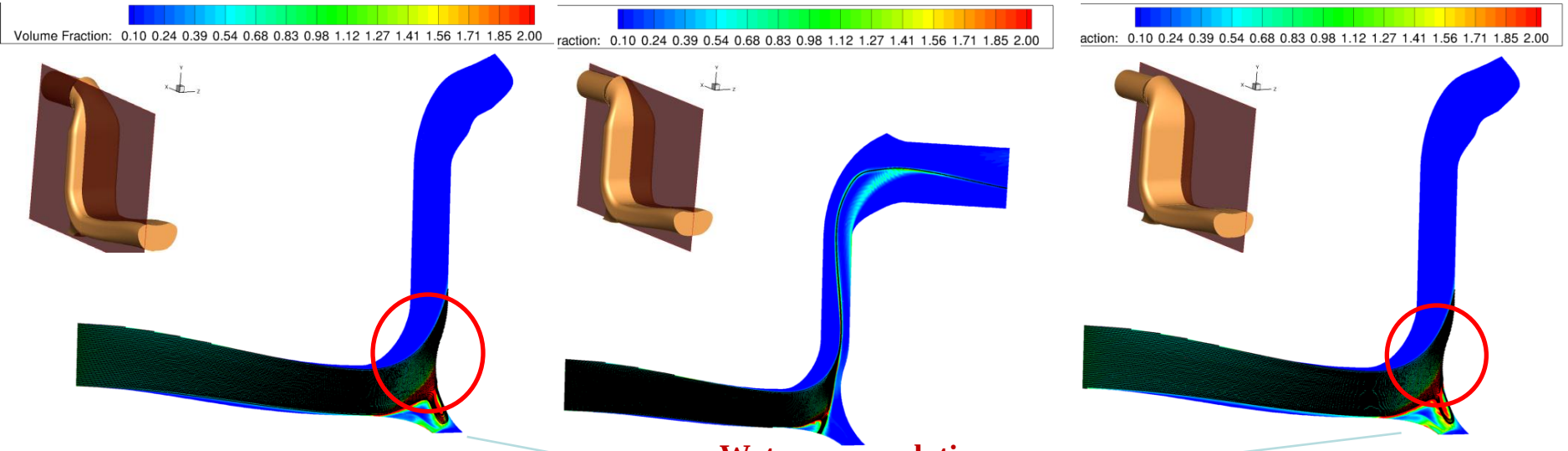

Water accumulation due to recirculation

Full 3D trajectories

Water volume fraction

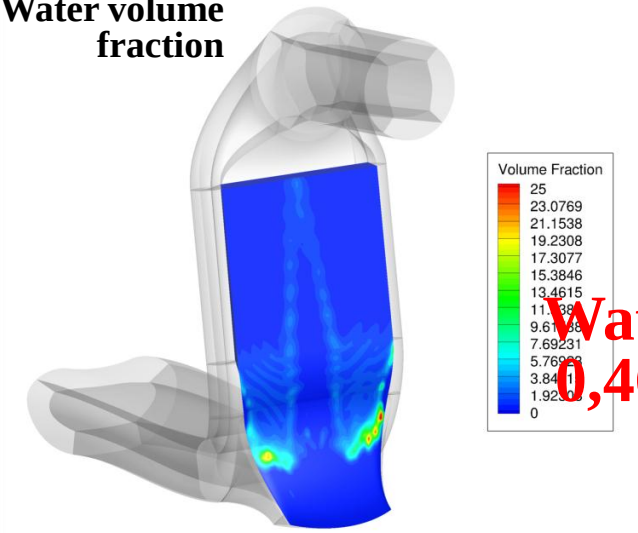

outlet water MFR / *inlet water MFR*	7.1 %

Water catch efficiency 92,9%
0,46 Kg/h at compresso inlet
85 g in 33 Km

Mathematical formulation

Finite volume method (FLUENT) : energy equation

$$\frac{\partial(\rho E)}{\partial t} + \nabla \cdot [\vartheta(\rho E + p)] = \nabla \cdot \left[k_{eff} \nabla T - \sum_j h_j J_j + (\tau \cdot \vartheta) \right] + S_h$$

Scalar transport equation on the surface on the nacelle

$$\nabla^2 T + \frac{\dot{q}}{k} = \frac{1}{\alpha} \frac{\partial T}{\partial t}$$

Radiative heat transfer equation for an absorbing, emitting and scattering medium as described hereafter

$$\frac{dI(\vec{r},\vec{s})}{ds} + (a + \sigma_S) I(\vec{r},\vec{s}) = an^2 \frac{\sigma T^4}{\pi} + \frac{\sigma_S}{4\pi} \int_0^{4\pi} I(\vec{r},\vec{s}) \Phi(\vec{s},\vec{s}') d\Omega'$$

The Discrete Ordinates (DO) radiative model has been selected to solve the radiation intensity : solving the Radiative Transfer Equation for discrete solid angles.

Gennaro Serino (g.serino@cira.it)

Geometry and meshing strategy

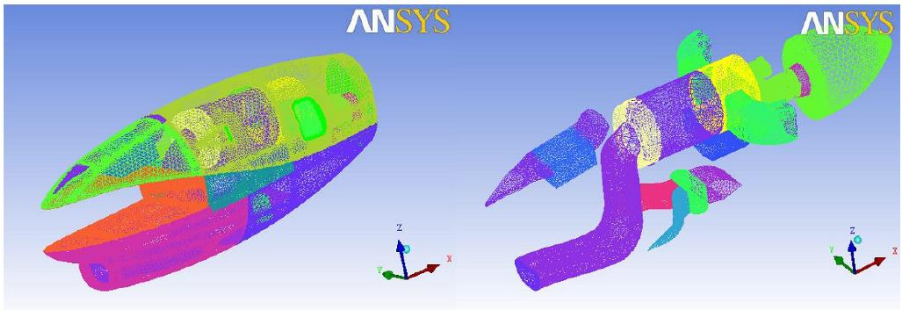

Nacelle (left) and internal (right) unstructured mesh on the engine

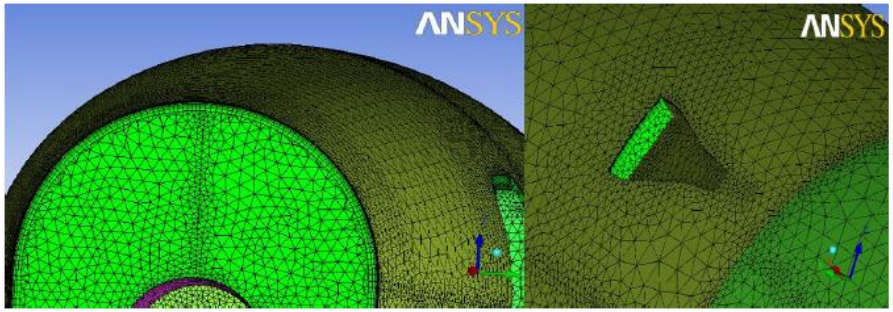

Details of the surface mesh on the nacelle : boundary layer (left) and NACA inlet (right)

Simplification and meshing approach

- **ICEM CFD to obtain the mesh**
- **5×10^6 elements for the external simulations after a first mesh sensitivity analysis on three less refined grids**
- **For the internal case, a 2×10^6 unstructured mesh has been used after the same refinement approach applied for the external field.**

Gennaro Serino (g.serino@cira.it)

ENGINE INTEGRATION
EM-11C ORKA CASE STUDY

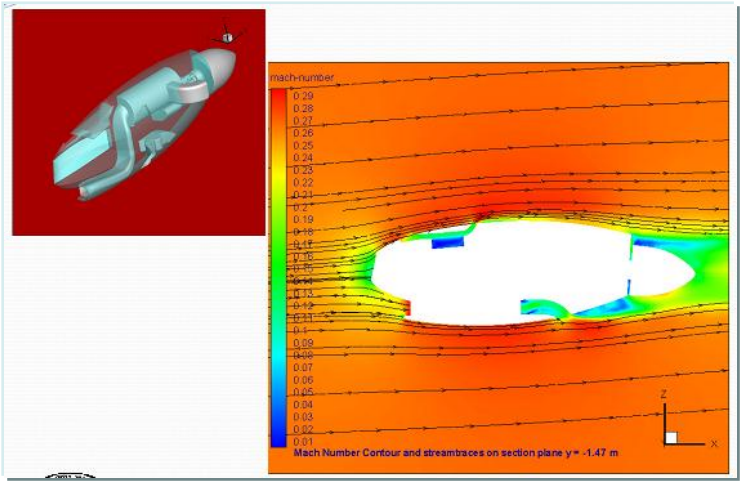

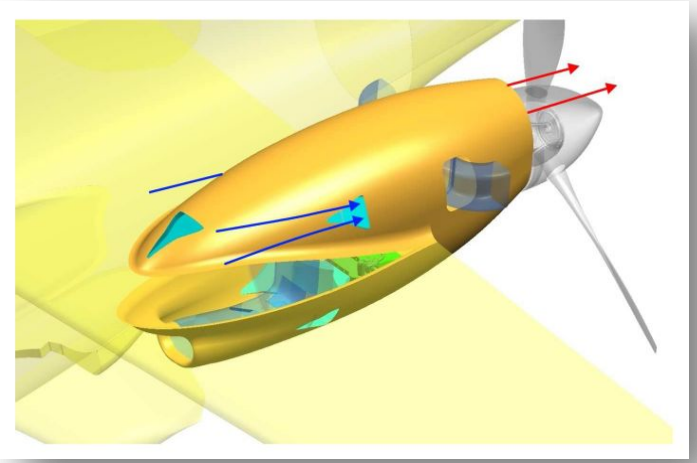

- ✓ **Flow and thermal field coupled**
- ✓ **Both internal and external flow**
- ✓ **Both convective and radiative heat transfer**
- ✓ **Assigned wall thickness and materials**
- ✓ **Real aircraft engine geometry**

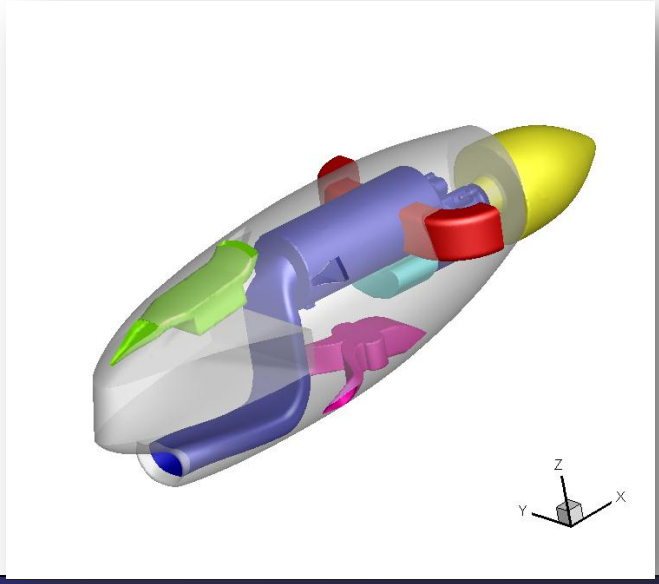

ENGINE INTEGRATION
EM-11C ORKA CASE STUDY

CIRA performed a conjugated heat trasfer study for the BE1 pusher nacelle ventilation evaluation

- ✓ **Analysis with and without radation effect**

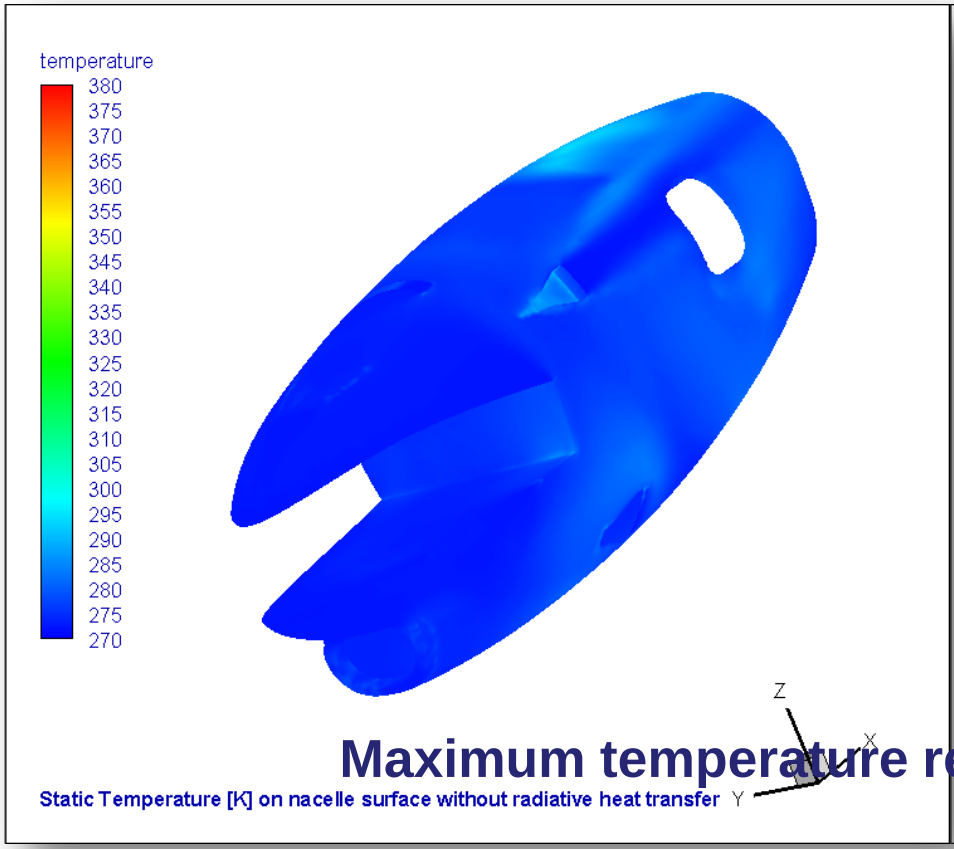

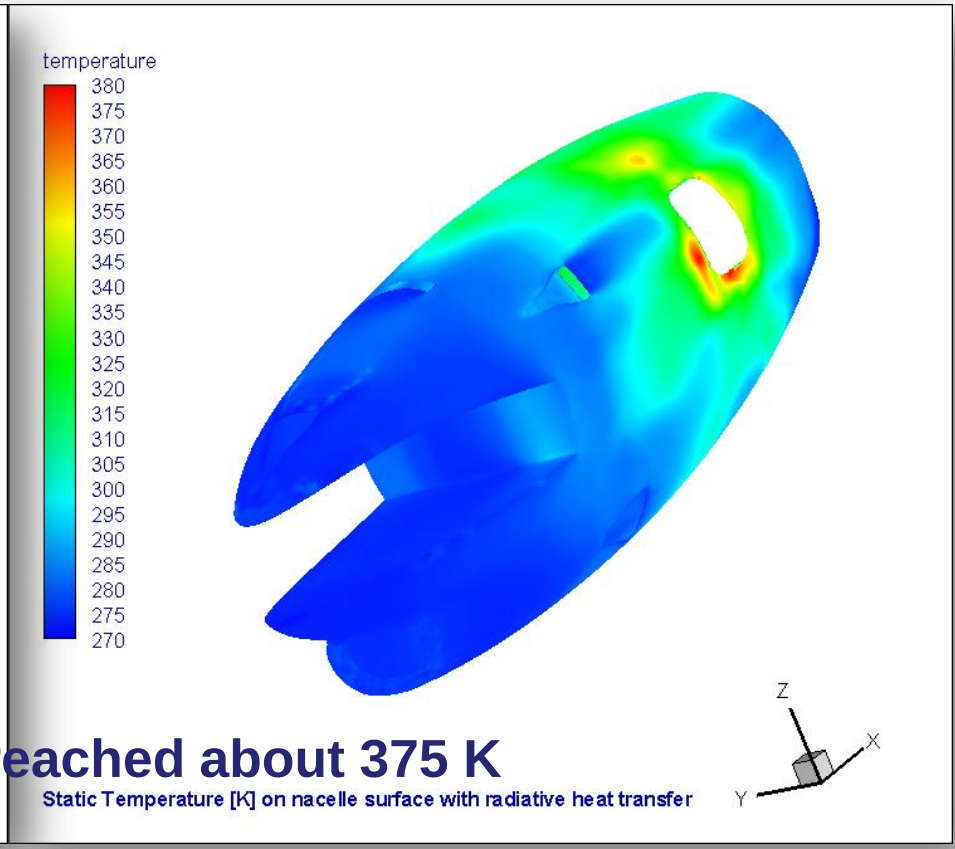

Maximum temperature reached about 375 K

CASE STUDY: NLF BUSINESS JET DESIGN

- The “principle of cosine” is used to analyze a 3D swept wing using a two-dimensional tool.
- A 3D boundary layer code coupled to a stability analysis method able to estimate the transition location in presence of crossflow is used to take into account the sweep effect on flow laminarity.
- Multiple constraints an design points are taken into account in the optimization.

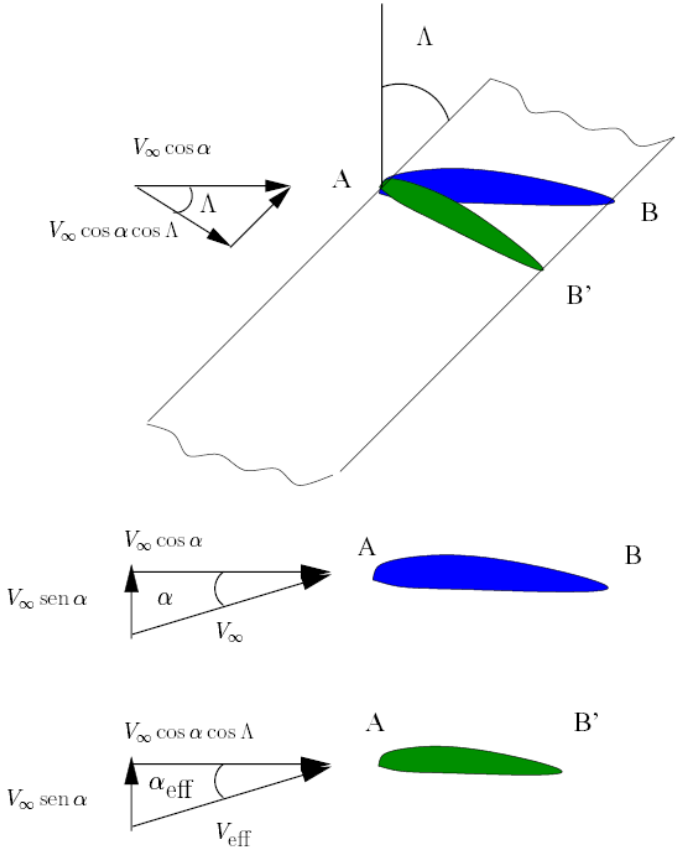

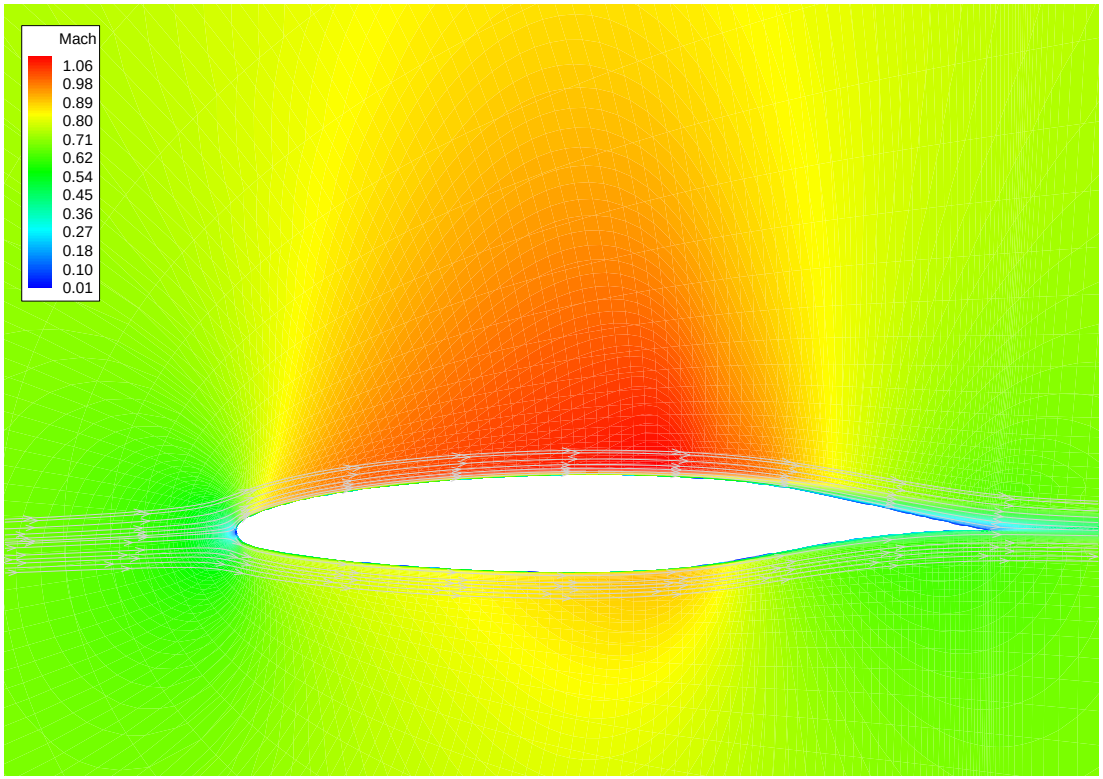

Detail of base airfoil design and verification

	Mach	Cl	Reynolds	Ncr	Cm max	Cd min	Transition
Design point 1	0.7	0.63	9e6	8	-	55dc	free
Design point 2	0.75	0.55	9e6	8	- 0.11	-	free
Design point 3	0.75	0.4	9e6	8	- 0.11	40dc	free
Design point 4	0.78	0.5	9e6	8	- 0.13	55dc	Fixed 60%

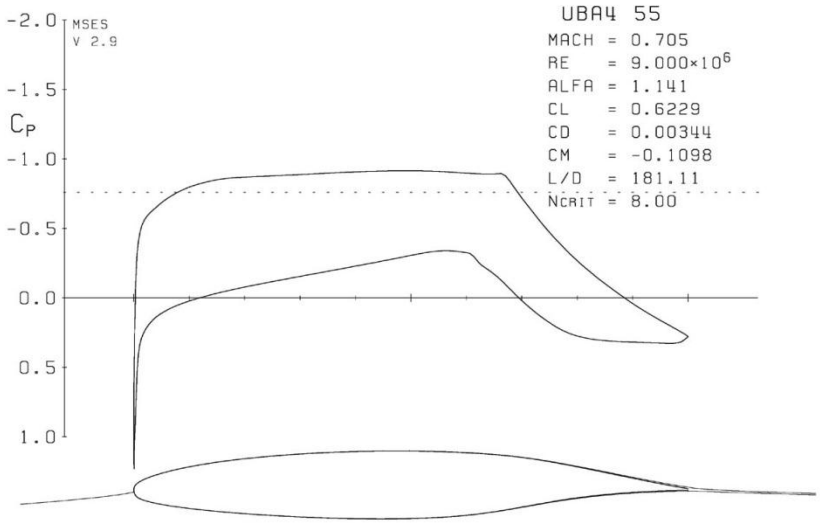

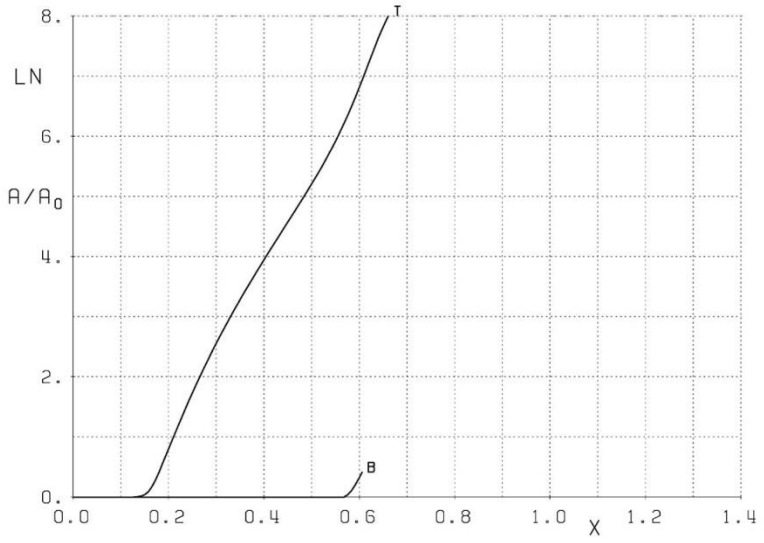

Tunnel test session

CIRA PT1:

Closed-circuit, pressurised transonic wind tunnel

(Mach = 0.35 - 1.1, Re 2 millions)

Polars, Cp, transition free and fixed:

Mach 0.6 - 0.82, Re 1.8e6 - 2.2e6

Tunnel test session

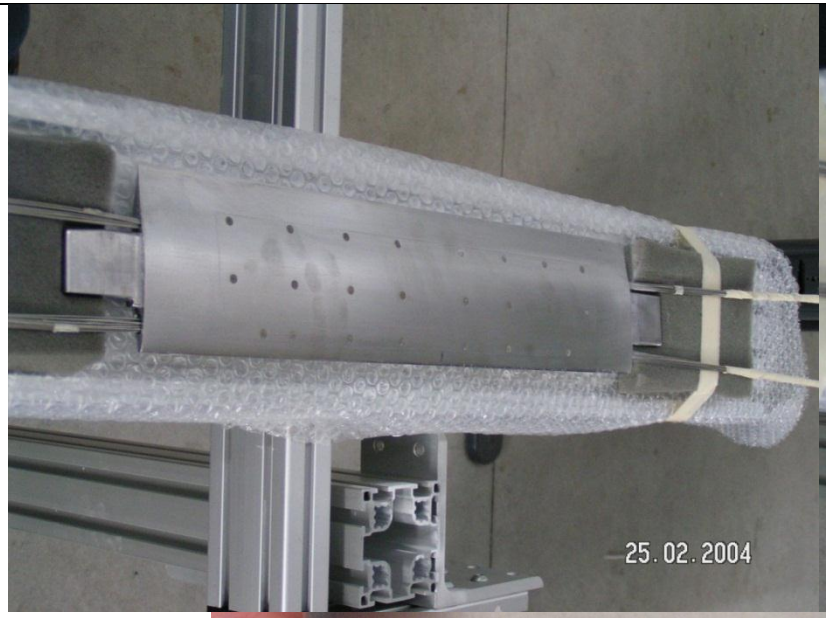

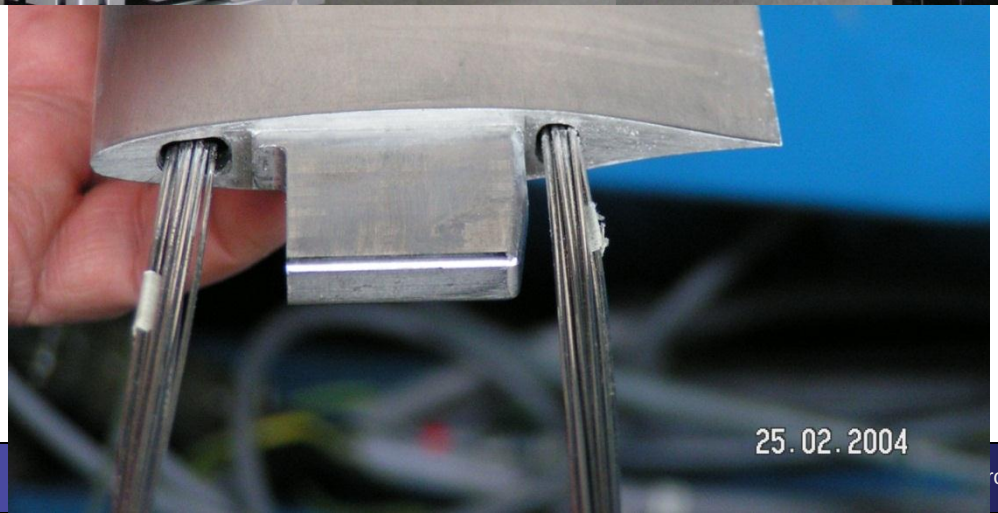

Tunnel test session

Example of transition visualization

CASE STUDY: NLF BUSINESS JET DESIGN

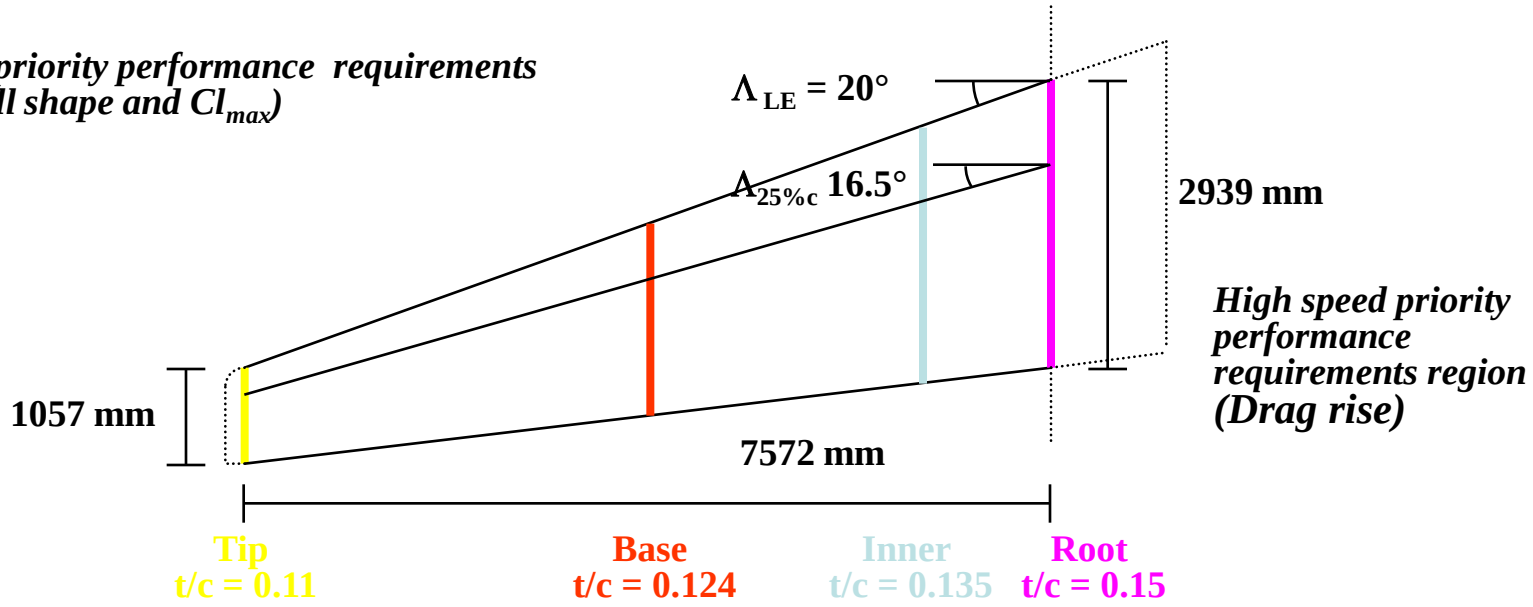

Constraints:

root incidence < 3° at Mach 0.75, C_L = 0.4

single curvature upper panel

straight trailing edge between 30% and 100% of b/2

Box volume > 4.5 m^3

thickness of root section > 14% for weight requirements

Design speed:
Mach cruise = 0.75 (C_L = 0.4 - 0.5)
MMO = 0.78

OPTIMIZATION

- Euler-2,5D B.L. ,transition Data-Base method coupling – Hybrid genetic algorithm coupling
- Twist, thickness optimization
- Root, tip optimization
- Navier-Stokes verification in high and low speed
- Linear stability analysis verification

CASE STUDY: NLF BUSINESS JET DESIGN

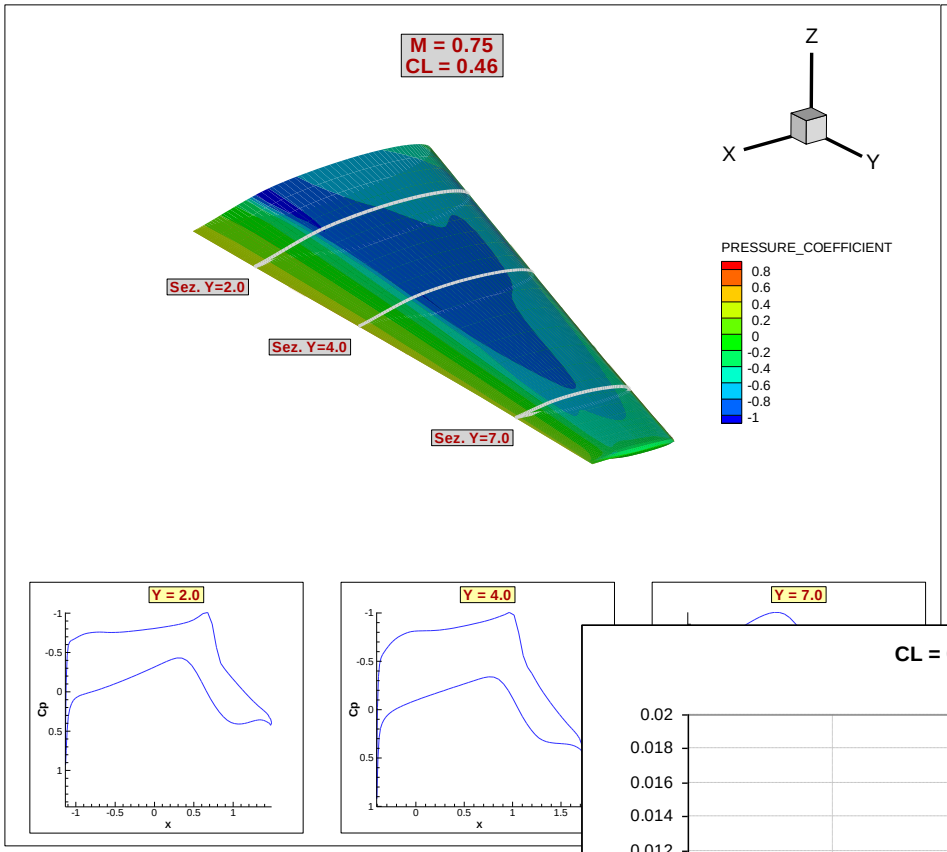

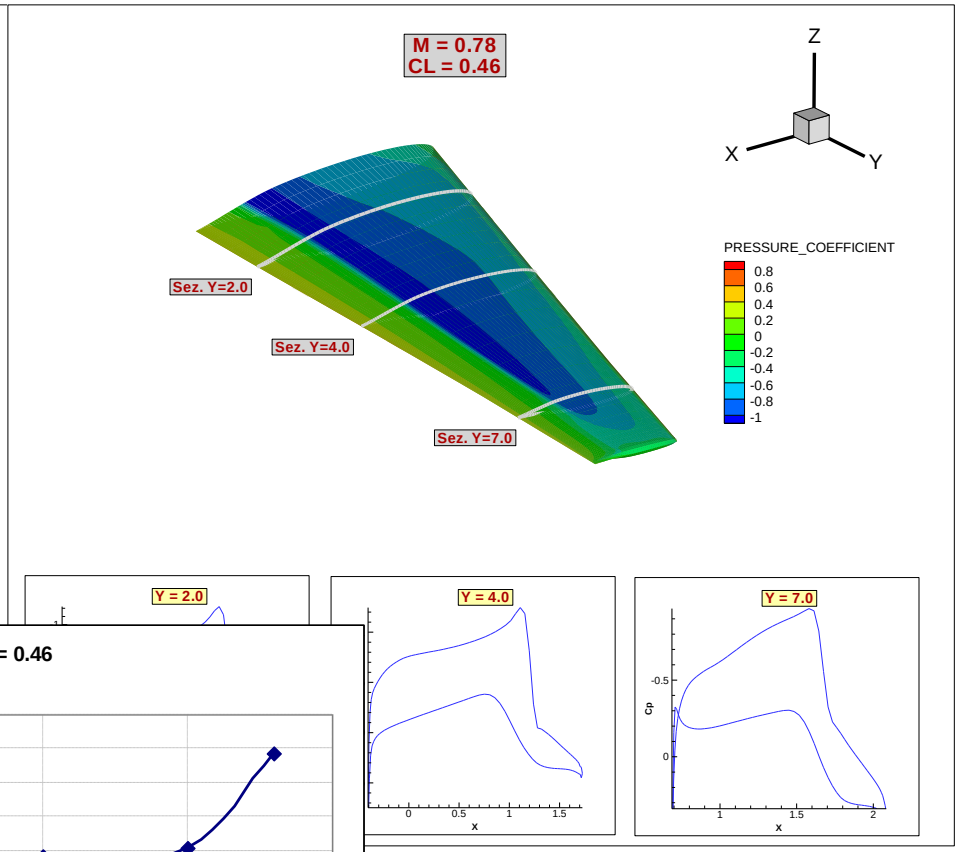

Experimental verification

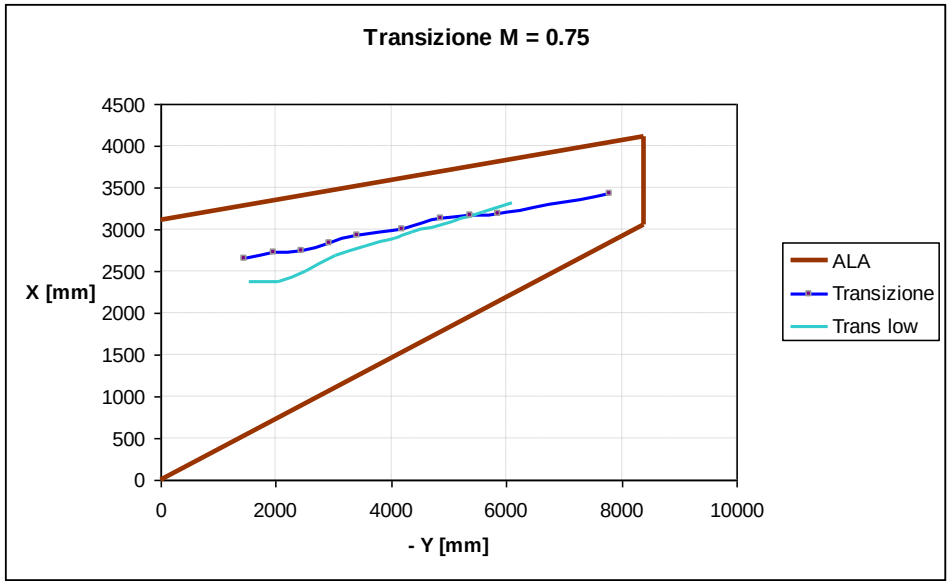

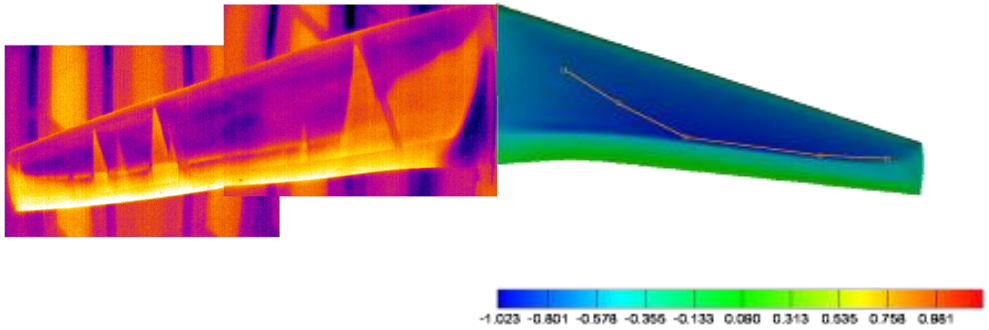

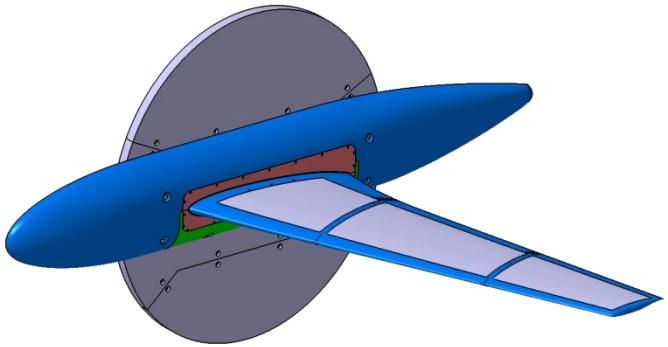

EUROLIFT (1999 – 2002)
European High Lift Programme

EUROLIFT
European Hight Lift Programme

Assessment & Improvement of CFD tools in the prediction of high-lift flow phenomena

- Capabilities to predict performance, stall behavior, flap setting and *Re* effects
- Capability to predict transition position and behavior as function of *Re* number
- Development of specific techniques for low-Mach flows (*e.g.*, low-speed preconditioning)
- Development of non-linear RANS turbulence modeling
- Applications to both 2D and 3D high-lift configurations

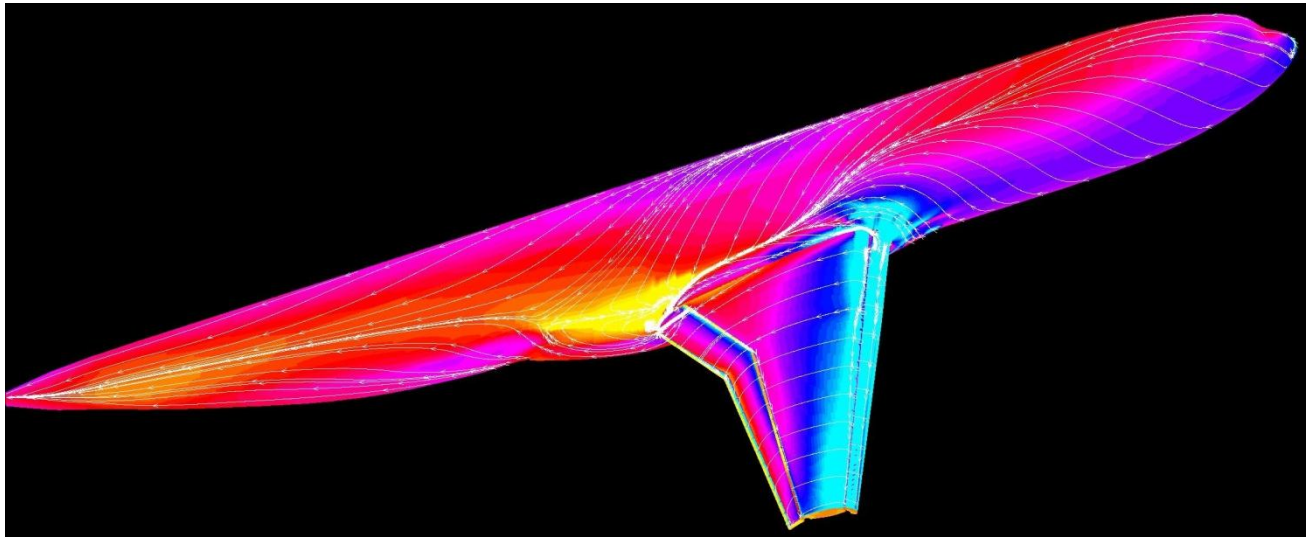

EUROLIFT II (2004 – 2007)
European High Lift Programme II

EUROLIFT II
European High Lift Programme

Further assessment & Improvement of CFD tools in the prediction of high-lift flows

- Introduction of laminar-turbulent transition effects into 3D CFD simulations
- Automatic CFD- based numerical optimization of 2D flap and WT testing
- Improve physical modeling of 3D stability and laminar-turbulent transition process

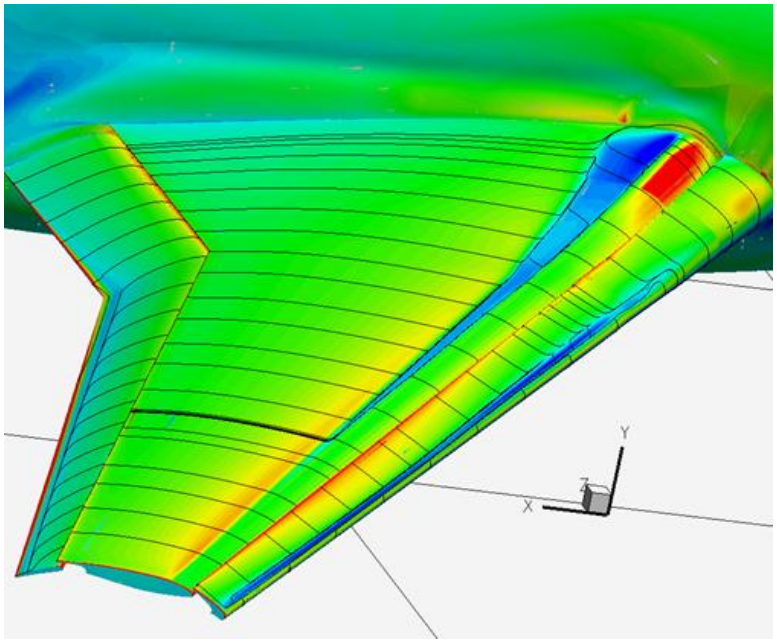

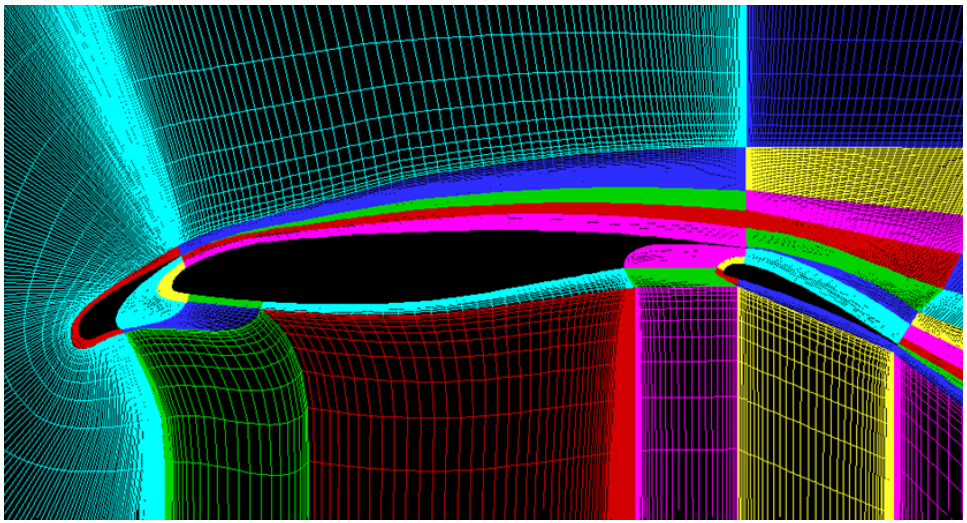

DeSiReH (2009 – 2013)

Design, Simulation and Flight Reynolds Number testing for advanced High Lift Solutions

Numerical optimization & prediction of unsteady high-lift flow phenomena

- 2D Multi-objective optimization of slat & flap at takeoff and landing conditions
- 3D automatic CFD- based numerical optimization of high-lift system for NLF wing
- Improvement of CFD tools for unsteady 3D calculations at and beyond stall conditions

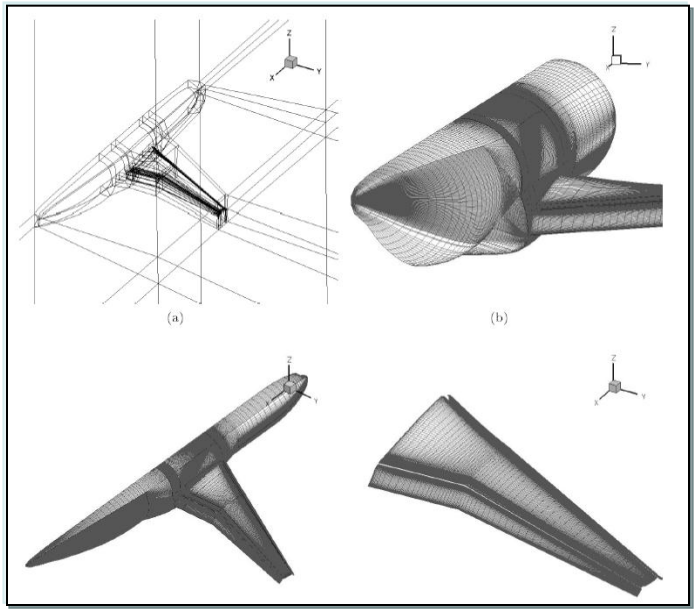

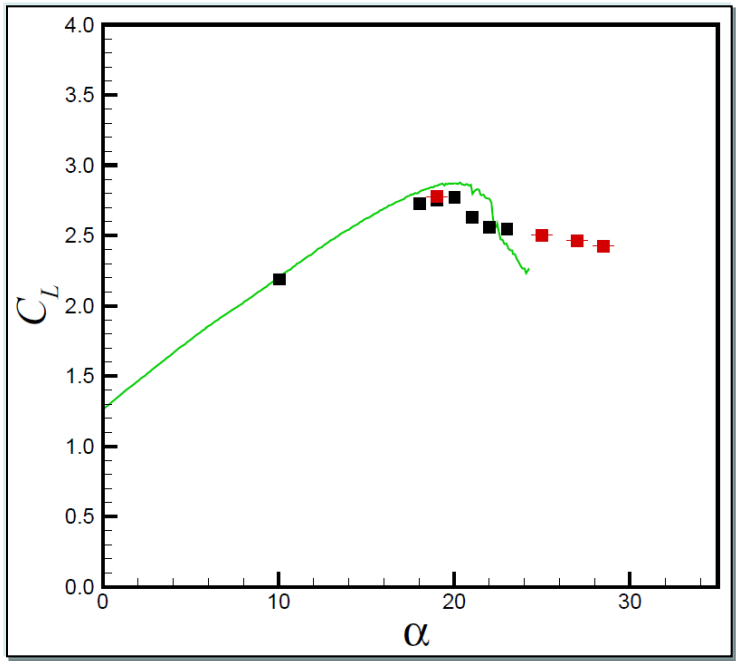

CFD Analysis and Design

DeSiReH: Bi-objectives optimization of flap/slat settings and shape at Takeoff & Landing conditions

Automatic geometry handling (elements' positioning and shape modification)

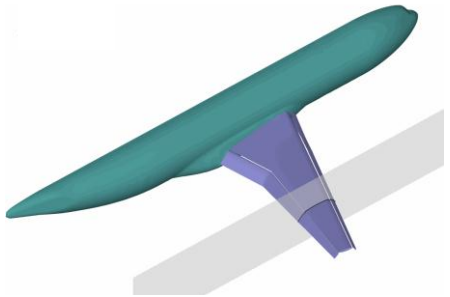

Automatic (parametric) grid generation at extreme elements' positions

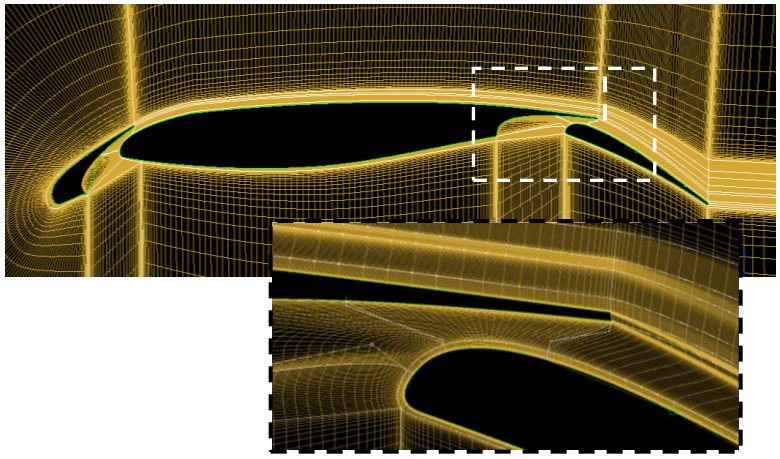

Genetic Algorithm Optimizer

Automatic CFD analysis

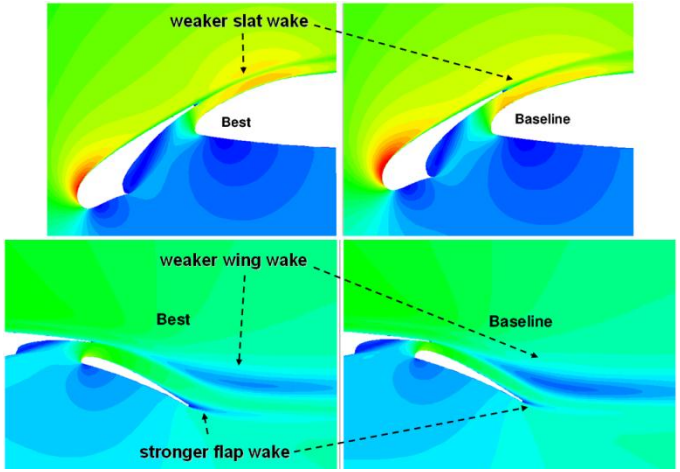

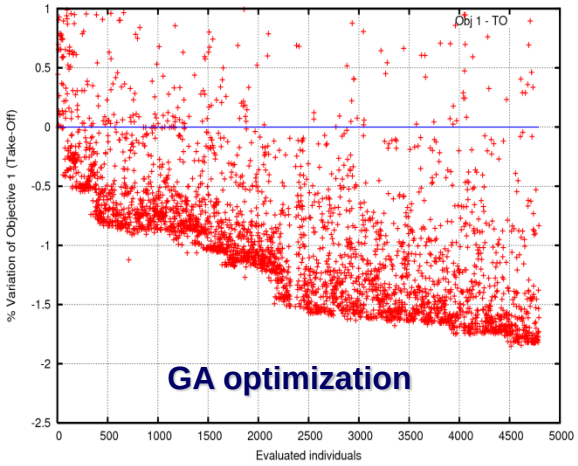

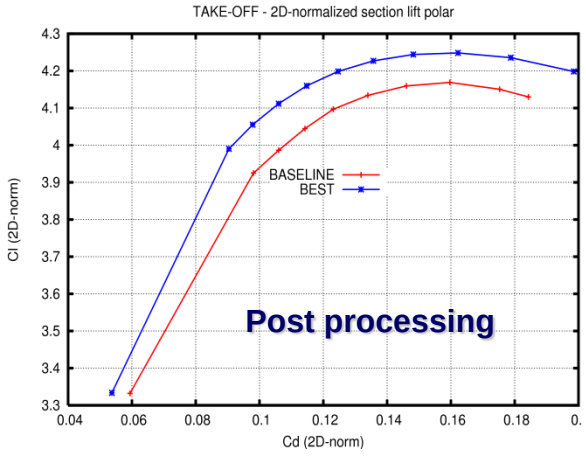

TECNOLOGIE AERODINAMICHE

- ✓ OGGI L'AERODINAMICA E' UNA TECNOLOGIA RELATIVAMENTE MATURA
- ✓ ESISTONO MOLTI SOFTWARE DISPONBILI SIA COMMERCIALMENTE CHE DI PUBBLICO DOMINIO
- ✓ NONOSTANTE I GROSSI PROGRESSI NELLE POTENZE COMPUTAZIONALI ANCORA NON E' PENSABILE UTILIZZO DI SOLUZIONI ESATTE (DNS) IN AMBITO PROGETTUALE
- ✓ I FLUSSI SEPARATI RAPPRESENTANO ANCORA UN'AERA CRITICA
- ✓ I SISTEMI DI FLOW-CONTROL ANCORA NON SONO MATURI PER UN UTILIZZO OPERATIVO
- ✓ LA PROSSIMA FRONTIERA E' LA MULTIDISCIPLINARITA'